

Aalto University

School of Electrical Engineering

Degree Programme in Electronics and Electrical Engineering

Pekka Järvinen

Pulse-width requirements in context with different modulation strategies of two- level 3-phase inverters

Master's Thesis

Espoo, October 23, 2014

Supervisor: Professor Ilkka Tittonen

Advisor: Samuli Heikkilä M.Sc. (Tech.)

Author:	Pekka Järvinen	
Title:	Pulse-width requirements in context with different modulation strategies of two-level 3-phase inverters	
Date:	October 23, 2014	Pages: viii + 73
Major:	Micro- and nanosciences	Code: S3010
Supervisor:	Professor Ilkka Tittonen	
Advisor:	Samuli Heikkilä M.Sc. (Tech.)	
<p>The purpose of this master's thesis is to review common pulse-width modulation strategies, introduce pulse-width limitations and present how pulse-width limitations affect the switching waveform of a power converter. The different factors determining the pulse-width limitations are identified and discussed.</p> <p>Several different factors are identified and methods are suggested for determining their impact on the final pulse-width limitations of the power converter. It is suggested that the limitations are separated into two categories. The first category contains internal, power converter specific limitations, which are determined at the factory. The second category contains external, load specific limitations, which are determined at installation site. The greater of these two is then used as the final pulse-width limitation.</p> <p>The effect of pulse-width limitations on the output of the power converter is analysed in both time and frequency domain. The pulse-width limitations are found to have several detrimental effects on the output of the power converter. The thesis also presents a general overview of the spectra of several modulation strategies.</p>		
Keywords:	Modulation, Variable frequency converter, Pulse-width limitations, two-level 3-phase inverter	
Language:	English	

Aalto-yliopisto

Sähkötekniikan korkeakoulu

Elektroniikan ja sähkötekniikan koulutusohjelma

DIPLOMITYÖN

TIIVISTELMÄ

Tekijä:	Pekka Järvinen		
Työn nimi:	Pulssirajoitukset kaksitaso 3-vaihe invertterien moduloinnissa		
Päiväys:	23. lokakuuta 2014	Sivumäärä:	viii + 73
Pääaine:	Mikro- ja nanotieteet	Koodi:	S3010
Valvoja:	Professori Ilkka Tittonen		
Ohjaaja:	Diplomi-insinööri Samuli Heikkilä		
<p>Tämän diplomityön tarkoitus on esitellä yleisiä pulssitaajuusmodulointistrategioita, esitellä pulssileveysrajoitukset ja tutkia, miten pulssileveysrajoitukset vaikuttavat taajuusmuuttajan kytkentäkuviioon. Tekijät, jotka vaikuttavat pulssileveysrajoituksiin, etsitään ja esitellään.</p> <p>Useita eri pulssileveysrajoituksiin vaikuttavia tekijöitä löydetään ja keinoja niiden määrittämiseksi esitellään. Työssä esitetään, että rajoitukset tulisi jakaa kahteen kategoriaan. Ensimmäinen kategoria sisältää taajuusmuuttajan sisäisistä ilmiöistä aiheutuvat rajoitukset, jotka voidaan määrittää tehtaalla. Toinen kategoria sisältää taajuusmuuttajaan kiinnitetystä kuormasta aiheutuvat rajoitukset, jotka voidaan määrittää asennuspaikalla.</p> <p>Pulssileveysrajoitusten vaikutus taajuusmuuttajan ulostulosignaaliin analysoidaan sekä aika- että taajuustasossa. Työssä huomataan, että pulssileveysrajoitukset heikentävät taajuusmuuttajan ulostulosignaalia. Työ myös tarjoaa katsauksen useiden eri modulaatiostrategioiden spektriin.</p>			
Asiasanat:	Modulointi, Taajuusmuuttaja, Pulssileveysrajoitukset, Kaksitaso 3-vaihe invertteri		
Kieli:	Englanti		

Acknowledgements

First of all I would like to express my gratitude to my advisor Samuli Heikkilä for the useful comments, remarks and engagement through the entire learning process of this master's thesis. Furthermore I would like to thank Professor Ilkka Tittonen for supervision of the thesis writing process.

I'm also grateful to everyone who supported me during the long days and nights of writing this thesis. Without your help completing this work would have been far more tedious.

Finally, I appreciate the financial support from ABB that funded this master's thesis.

Espoo, October 23, 2014

Pekka Järvinen

Abbreviations and Acronyms

ABB	Asea Brown Boveri
CPWM	Continuous pulse-width modulation
D-MOSFET	Metal-oxide-semiconductor field-effect transistor with gate on top of the substrate
DPWM	Discontinuous pulse-width modulation
DPWM0	Discontinuous pulse-width modulation with 30° leading clamp
DPWM1	Discontinuous pulse-width modulation with zero clamp at voltage peak
DPWM2	Discontinuous pulse-width modulation with 30° lagging clamp
DPWM3	Discontinuous pulse-width modulation with 30° alternating clamp
DPWMMIN	Discontinuous pulse-width modulation using only lower zero vector
DPWMMAX	Discontinuous pulse-width modulation using only upper zero vector
dqo transform	Direct-quadrature-zero transform
DTC	Direct torque control
EM	Electromagnetic
GTO	Gate turn-off thyristor
HCC	Hysteresis current control
IGBT	Insulated gate bipolar transistor

IGCT	Integrated gate-commutated thyristor
l-l output voltage	line-to-line output voltage
MOSFET	Metal-oxide-semiconductor field-effect transistor
MPW	Minimum pulse-width
PCB	Printed circuit board
PWM	Pulse-width modulation
SVM	Space-vector modulation
SVPWM	Space-vector pulse-width modulations
U-MOSFET	Metal-oxide-semiconductor field-effect transistor with buried gate

Contents

Abbreviations and Acronyms	v
1 Introduction	1
2 Modulation	4
2.1 Modulation strategies	4
2.1.1 Carrier-based pulse-width modulation	6
2.1.2 Space-vector pulse-width modulation	10
2.1.3 Discontinuous pulse-width modulation	15
2.1.4 Hysteresis based modulation	17
2.2 Harmonic analysis	19
2.3 Minimum pulse-width limitations	23
3 Physical constraints	27
3.1 Inverter output bridge components	27
3.1.1 Switching semiconductors	28
3.1.2 Free-wheeling diodes	33
3.1.3 Gate driver limitations	35
3.2 DC circuit oscillations	36
3.3 Cable oscillations	37
3.3.1 Oscillation of the reflected wave	38
3.3.2 Pulse-width and cable oscillations	42

4	Modulation and pulse-width limitations	44
4.1	Time domain	45
4.1.1	Error caused by pulse-width limitations	46
4.1.2	Choosing the modulation approach	47
4.1.3	Double switching	50
4.1.4	Switching frequency	53
4.2	Output voltage spectrum	54
4.2.1	Modulation strategy and index	55
4.2.2	Pulse-width limitations	58
4.2.3	Double switching elimination	61
5	Conclusions	65
A	Park's transform	71

Chapter 1

Introduction

Power electronics involves the study of electronic circuits intended to control the flow of electrical energy. These circuits handle power flow at levels much higher than the individual device ratings. While in the past the focus of the field has been on electronic devices, which can handle high power levels, over the past few decades it has transitioned into an applications-driven field.

Modulation is one of the most important single processes involved in power electronics. It is defined as the process of switching electronic devices within power electronic converters from one state to another. There are only two allowable states for the electronic devices within a power electronic converter: fully on and fully off. However, a multitude of different strategies for the order and frequency of these state changes exists. Different modulation strategies affect parameters such as switching frequency, distortion, losses, harmonic generation and speed of response. This makes it important to fully understand the application of the power converter device when choosing the right modulation strategy for the given situation. [1]

Modern power converters utilize modulation, because the precise switching process allows the converter to convey exactly the right amount of power to the connected device. This way, it is possible to approach extremely high, close to unity, rates of electrical efficiency. In the past linear regulators were used instead of devices based on switching. In linear regulators the differ-

ence between the input and regulated voltages is dissipated as waste heat. Switching power converters therefore can yield a much larger efficiency than their non-switching counterparts.

A three-phase inverter has three power poles as depicted in figure 1.1. Each power pole consists of an ideal switch switching the DC-rail according to a modulation process. These state changes directly affect the output of the inverter. It should be noted, however, that in reality the power pole is generally realized using a buck and a boost converter containing two switching semiconductors and two protecting diodes, because the concept of an ideal switch is purely theoretical. However, this only applies to a two-level inverter. In multilevel converters the number of semiconducting switches is higher. The pair of switching semiconductors in the buck and boost converters are ideally complementary, but it is later noted that in reality this is impossible. Therefore the modulation process has to control a total of six switches. [2]

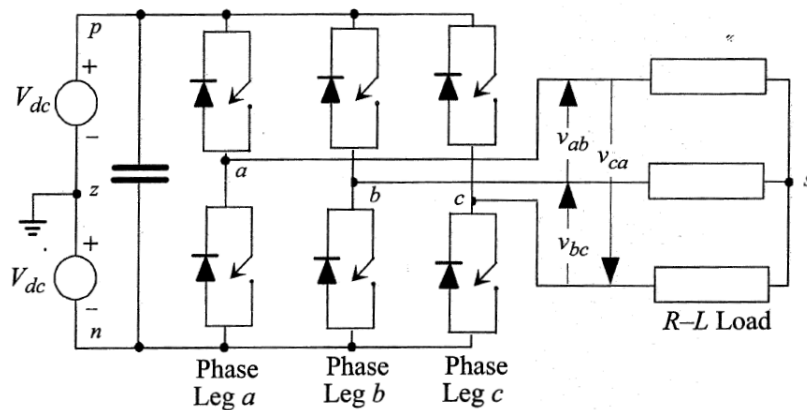


Figure 1.1: Two-level three-phase inverter consists of three power poles, which are switched based on a modulation strategy [1].

The purpose of this thesis is to first review the theoretical background of modulation and control methods in the context of two-level three-phase inverters and then introduce the concept of minimum pulse width limitations into the present modulation strategies. Then, the different physical con-

straints determining the limitations are discussed. Finally the thesis presents the effect of the minimum pulse-width limitations on the output signal of the inverter. The study is based on computer simulations using a special software written for this purpose.

Chapter 2

Modulation

This chapter will discuss the theoretical background behind modulation strategies and minimum pulse-width limitations. The discussion in this chapter stays on the abstract level without giving detailed description, how the actual components affect the operation power converters.

The basic modulation strategies will be examined starting from the earliest implementation of pulse-width modulation and ending with the more modern discontinuous and state-vector based modulation strategies. After the modulation strategies are explained, the concept of minimum pulse-width limitations is introduced and discussed. A method for analysing the spectrum of different modulation methods analytically is reviewed.

2.1 Modulation strategies

As discussed in chapter 1 modulation is the process of switching the state of electronic devices within power electronic converters from one state to another. It was mentioned, that there are numerous different modulation methods. The modulation methods can be divided into two categories, which are carrier-based and hysteresis-based. The carrier-based modulation methods are discussed first followed by the hysteresis-based modulation methods.

By definition all modulation schemes create trains of switched pulses,

which have the same fundamental volt-second average as a target reference waveform at any instant. However, these trains of switched pulses also contain unwanted harmonic components. Hence, the primary objective of any modulation strategy is to calculate the converter switch on times which create the desired target output voltage or current. The secondary objective is then to determine the most effective way of arranging the switching process to minimize unwanted harmonic distortion, switching losses or any other performance criterion. [1]

Pulse-width modulation (PWM) has a long history starting with the historic paper on sinusoidal PWM published by A. Schönung et al. in as early as 1964. From the beginning a great number of algorithms have been optimized for different situations. Early PWM research efforts focused on increasing the available output range. As the theory became more developed, the slow switching properties of thyristors became the limitation for minimum and maximum pulse-widths. [3]

In ideal PWM both switches of the power pole are complementary and switched at the same time. However, in reality the logic is not exactly complementary due to the natural differences the separate discrete components have. Therefore a small delay must be added to the switching sequence in order to prevent the semiconducting components from conducting at the same time and thereby short circuiting the DC-rail. This delay is called the dead-time or dwell-time, T_d . The dead-time provides a safety zone, which allows for device-dependent effects to be mitigated. [1] From the definition of the ideal PWM it instantly follows that it is an efficient way of controlling the amount of power delivered to a load without dissipating any wasted power.

In applications of the earlier defined modulation methods the system often incorporates an appropriate low-pass filter. For example when PWM is used to control the speed of a fan, the inertia and inductance of the system itself act as a low-pass filter. When it is used to control the brightness of a light-emitting diode, the human eye acts as a low-pass filter.

2.1.1 Carrier-based pulse-width modulation

The operation of the earliest and most straightforward modulation strategy is presented in figure 2.1. It is termed naturally sampled PWM. The low frequency reference signal (usually a sinusoid) is compared against a high-frequency carrier waveform. The carrier waveform is arbitrary, but usually either a sawtooth wave or the presented triangular wave. Whenever the two signals cross the value of the carrier waveform of the resulting PWM-wave changes. The resulting PWM-signal then represents directly the switching state within the power converter. To obtain a sinusoidal output using this modulation strategy, the reference waveform has the following form

$$\nu_{az}^* = M \frac{V_{DC}}{2} \cos \omega_0 t, \quad (2.1)$$

where m is the modulation index or modulation depth with range $0 < M < 1$, ω_0 is the target output frequency and θ_0 is an arbitrary output phase. For a three-phase modulation the process described earlier is repeated for each of the three phases yielding three PWM-signals as presented in figure 2.2. [1]

The fundamental line-to-line (l-l) output voltage for a three-phase power converter are given by the differences between the phase leg voltages.

$$\nu_{ab}^* = \nu_{az}^* - \nu_{bz}^* = M \sqrt{3} \frac{V_{DC}}{2} \cos(\omega_0 t + \frac{\pi}{6}) \quad (2.2)$$

$$\nu_{bc}^* = \nu_{bz}^* - \nu_{cz}^* = M \sqrt{3} \frac{V_{DC}}{2} \cos(\omega_0 t - \frac{\pi}{2}) \quad (2.3)$$

$$\nu_{ca}^* = \nu_{cz}^* - \nu_{az}^* = M \sqrt{3} \frac{V_{DC}}{2} \cos(\omega_0 t + \frac{5\pi}{6}) \quad (2.4)$$

It should be noted that the maximum reference magnitude for the modulation index of $M = 1$ is only $\sqrt{3} \frac{V_{DC}}{2}$, compared to the V_{DC} of a single-phase inverter. [1]

A major limitation with the naturally sampled PWM described above is the difficulty of its implementation in a modern digital modulation system, because the intersection between the reference sinusoid and the triangular or sawtooth carrier is defined by a transcendental equation and is complex to calculate. To overcome this limitation modern systems implement a "regular

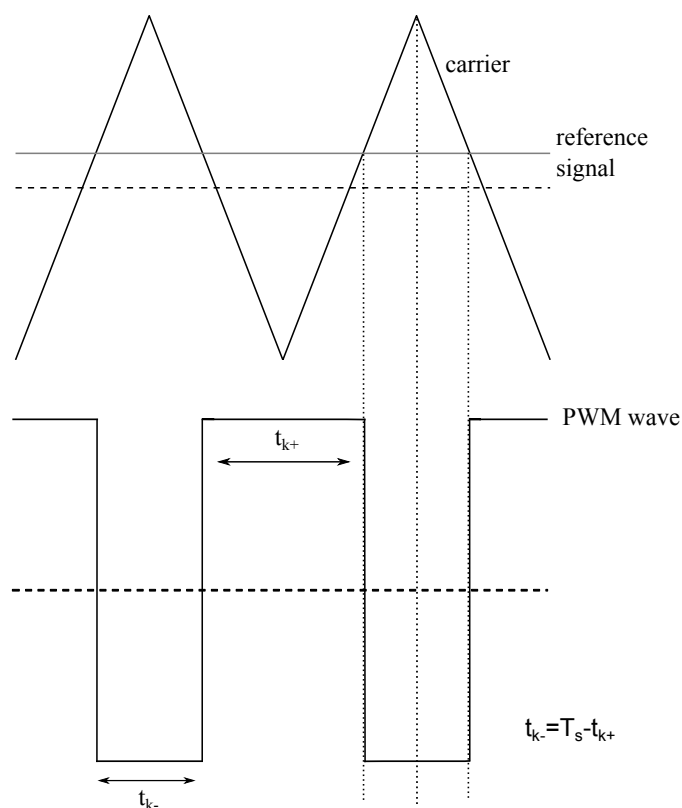


Figure 2.1: Two-level carrier based naturally sampled PWM. It can be seen that the resulting PWM-wave changes state whenever the reference signal crosses the carrier triangle wave. T_s is the duration of the switching cycle and t_{k+} and t_{k-} are the on and off state durations respectively.

sampled” PWM strategy, where the low-frequency reference waveforms are sampled and then held constant during each carrier interval as presented in figure 2.3. From this figure it can also be seen that the sampling process produced a stepped reference waveform which is phase delayed with respect to the original reference waveform. This phase delay can be compensated by phase advancing the reference waveform. [1]

As discussed earlier, another major limitation in the concepts of three-phase inverter modulation is the reduced maximum peak fundamental output l-l voltage of $\sqrt{3}\frac{V_{DC}}{2}$. This limitation is especially problematic for motor drive

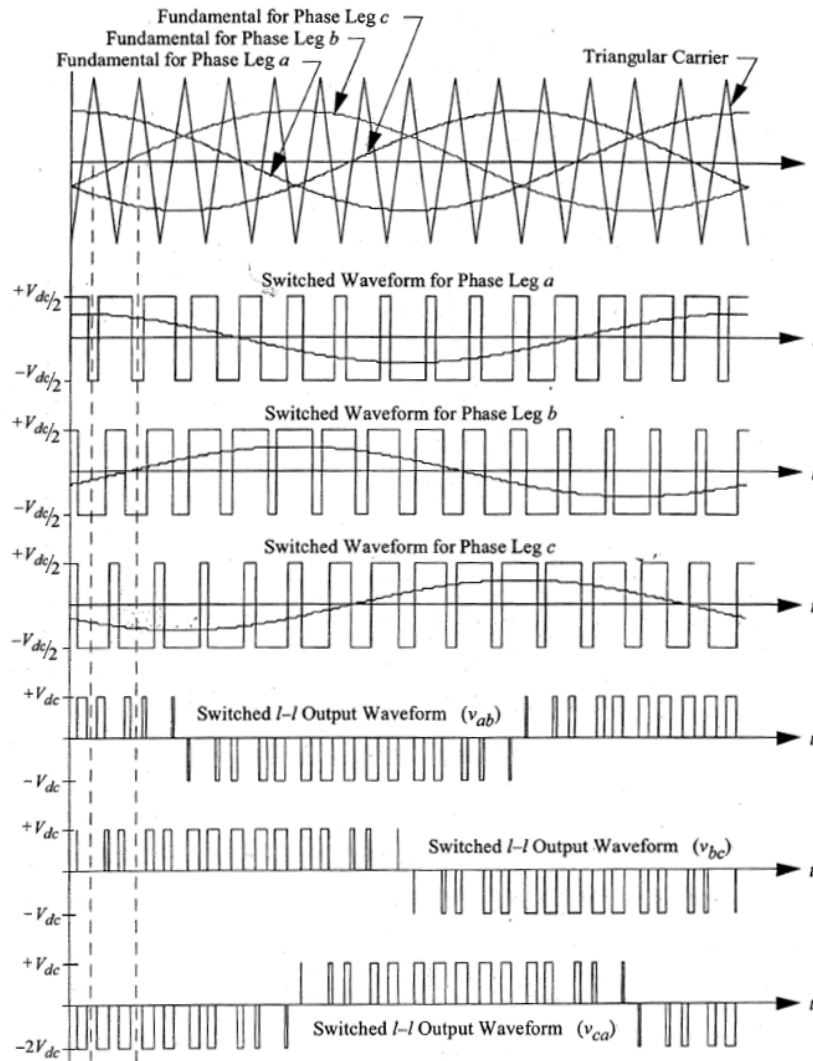


Figure 2.2: Naturally sampled PWM for a three phase inverter. The modulation process yields a separate PWM-signal for each of the phases. [4]

applications. A motor has to run at its rated volts per hertz to sustain rated load torque without overheating. However, since the average rectified DC link voltage is $\frac{3V_p}{\pi}$ assuming a perfect zero impedance source and rectifier operating in continuous conduction, the maximum peak inverter output voltage will be $\frac{\sqrt{3}}{2} \frac{3V_p}{\pi}$ or 82.7 % of V_p . This means that on the output side the PWM inverter will only be capable of about 83 % of rated power. [1]

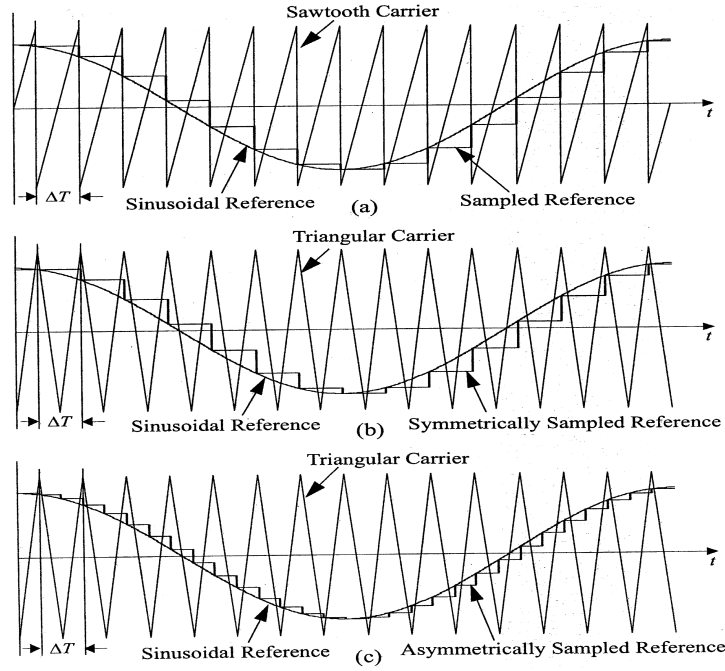


Figure 2.3: Modern systems implement a "regular sampled" PWM, where the low-frequency reference waveforms are sampled and then held constant during each carrier interval [1].

Beginning as early as in 1975, it has been recognized that maximum modulation index of a three-phase inverter PWM system can be increased if a common mode third-harmonic term is injected into the target reference waveform of each phase leg. If the 3rd harmonic is injected into the sinusoidal $\frac{2\pi}{3}$ displaced references the following set of equations emerges.

$$v_{az}^* = \frac{V_{DC}}{2} [M \cos \omega_0 t + M_3 \cos 3\omega_0 t] \quad (2.5)$$

$$v_{bz}^* = \frac{V_{DC}}{2} [M \cos(\omega_0 t - \frac{2\pi}{3}) + M_3 \cos 3\omega_0 t] \quad (2.6)$$

$$v_{cz}^* = \frac{V_{DC}}{2} [M \cos(\omega_0 t + \frac{2\pi}{3}) + M_3 \cos 3\omega_0 t] \quad (2.7)$$

By dividing through by $M \frac{V_{DC}}{2}$ the equations above can be written in the form $\nu = \cos \theta_0 + \gamma \cos 3\theta_0$, where $\gamma = \frac{M_3}{M}$ represents the parameter to be optimized to reduce the maximum value of the function as much below unity as possible. It turns out that $\gamma = -\frac{1}{6}$ produces the optimum value, which

yields the following result.

$$\nu_{az,max} = \frac{\sqrt{3}}{2} M \frac{V_{DC}}{2} \quad (2.8)$$

Hence the modulation index M can now increase to $\frac{2}{\sqrt{3}}$ before $\nu_{az,max}$ reaches $\frac{V_{DC}}{2}$. [1] The injected harmonics are not visible in the resulting l-l voltages, which is clear by looking at equations 2.5, 2.6 and 2.7. When the equations are subtracted from each other, the 3rd harmonic term disappears. The injected harmonics are, thus, called the zero sequence signal $e_i(t)$ [4].

For a long period, carrier-based PWM methods were widely used in most applications. The earliest modulation signals for carrier-based PWM were sinusoidal. However, later the use of an injected zero-sequence signal for a three-phase inverter initiated the research for non-sinusoidal carrier-based PWM. Compared with sinusoidal three-phase PWM, it was shown that non-sinusoidal three-phase PWM can extend the linear modulation range for line-to-line voltages. [4] Carrier-based pulse-width modulation strategies can furthermore be divided into two categories: continuous (CPWM) and discontinuous (DPWM). [3] There are several different DPWM strategies and they will be discussed later in this thesis.

2.1.2 Space-vector pulse-width modulation

A space-vector is obtained by summing together the different instantaneous voltages of phases as vectors. In a symmetric three-phase system the phase difference between the phases is always 120° . This can be presented by various notations, most often the complex and vector notation. The complex representations of these phase-vectors, or phasors, is given below. Generally the coordinate system is chosen so, that the phasor \vec{a} points along the

direction of the magnetic axis of one of the stator windings.

$$\vec{a}^0 = 1 \quad (2.9)$$

$$\vec{a}^1 = e^{i\frac{2\pi}{3}} = -\frac{1}{2} + i\frac{\sqrt{3}}{2} = 1\angle 120^\circ \quad (2.10)$$

$$\vec{a}^2 = e^{i\frac{4\pi}{3}} = -\frac{1}{2} - i\frac{\sqrt{3}}{2} = 1\angle 240^\circ \quad (2.11)$$

Using this notation the stator current, for example, would get the form $\vec{i}_s = \frac{2}{3}(i_a + i_b\vec{a} + i_c\vec{a}^2)$. The multiplier $\frac{2}{3}$ makes the length of the space-vector equal to the maximum values of the phase quantities, which simplifies the calculations when applied to real electric machines. [5]

A different approach to PWM modulation is based on the space-vector representation of the voltages in the α, β plane. This approach is called space-vector modulation (SVM) The α and β components are found by Park's transform, which is also known as direct-quadrature-zero transform (dqo transform). In this transform the total power, as well as the impedances, remains unchanged assuming the impedances are symmetrical. Appendix A reviews this transform. The power converter switching states are represented by vector \vec{S} , for which there are 8 possible states as depicted in figure 2.4. From these eight states it is possible to define eight voltage vectors $\vec{U}_0 = \frac{2}{3}V_{DC}\vec{S}_0 = \frac{2}{3}V_{DC}[000], \dots, \vec{U}_7 = \frac{2}{3}V_{DC}\vec{S}_7 = \frac{2}{3}V_{DC}[111]$ corresponding to the switching states. The length of these voltage vectors is $\frac{2}{3}V_{DC}$ with the exception of vectors \vec{U}_0 and \vec{U}_7 whose length is zero. [4]

In one sampling interval, the output voltage vector \vec{U} can then be written as

$$\vec{U}(t) = \frac{t_0}{T_s}\vec{U}_0 + \frac{t_1}{T_s}\vec{U}_1 + \dots + \frac{t_7}{T_s}\vec{U}_7 \quad (2.12)$$

where t_0, \dots, t_7 are the turn-on times of the vectors $\vec{U}_0, \dots, \vec{U}_7$. According to linear geometry the vector \vec{U} can be decomposed into $\vec{U}_0, \dots, \vec{U}_7$ in infinitely many ways. However, in order to make full use of active turn-on time for space vectors the vector \vec{U} is commonly split into the two nearest adjacent voltage vectors and zero vectors \vec{U}_0 and \vec{U}_7 . For example in sector I vector

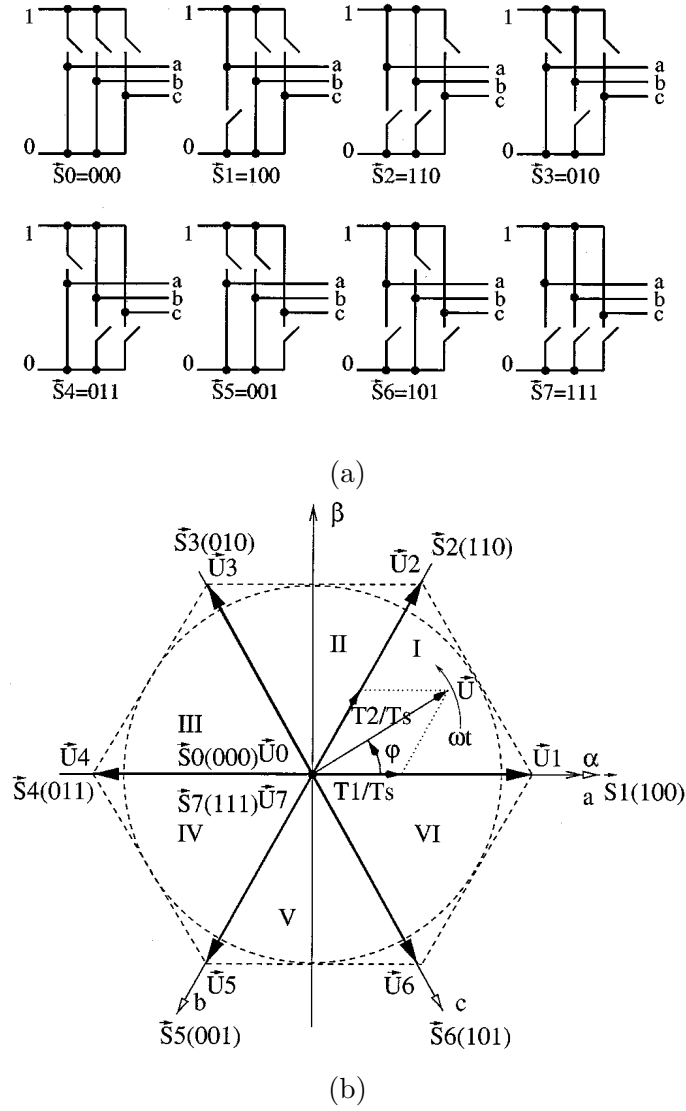


Figure 2.4: Figure 2.4a represents the physical switching states in a 3-phase inverter whereas 2.4b represents the voltage vector space in α and β coordinates. [4]

\vec{U} can be expressed as

$$\vec{U} = \frac{T_1}{T_s}\vec{U}_1 + \frac{T_2}{T_s}\vec{U}_2 + \frac{T_7}{T_s}\vec{U}_7 + \frac{T_0}{T_s}\vec{U}_0 \quad (2.13)$$

where $T_s - T_1 - T_2 = T_0 + T_7 \geq 0$, $T_0 \geq 0$ and $T_7 \geq 0$. The different values of variables T_1, \dots, T_6 needed for the decomposition of U in different sectors can be directly derived using the voltage vector space graph and they are

listed in table 2.1. [4]

Table 2.1: The switch on times T_1, \dots, T_6 as described in [4].

Sector I ($0 \leq \omega t \leq \frac{\pi}{3}$)	Sector II ($\frac{\pi}{3} \leq \omega t \leq \frac{2\pi}{3}$)	Sector III ($\frac{2\pi}{3} \leq \omega t \leq \pi$)
$T_1 = \frac{\sqrt{3}}{2} m T_s \cos(\omega t + \frac{\pi}{6})$	$T_2 = \frac{\sqrt{3}}{2} m T_s \cos(\omega t + \frac{11\pi}{6})$	$T_3 = \frac{\sqrt{3}}{2} m T_s \cos(\omega t + \frac{3\pi}{2})$
$T_2 = \frac{\sqrt{3}}{2} m T_s \cos(\omega t + \frac{3\pi}{2})$	$T_3 = \frac{\sqrt{3}}{2} m T_s \cos(\omega t + \frac{7\pi}{6})$	$T_4 = \frac{\sqrt{3}}{2} m T_s \cos(\omega t + \frac{5\pi}{6})$
$T_0 + T_7 = T_s - T_1 - T_2$	$T_0 + T_7 = T_s - T_2 - T_3$	$T_0 + T_7 = T_s - T_3 - T_4$
Sector IV ($\pi \leq \omega t \leq \frac{4\pi}{3}$)	Sector V ($\frac{4\pi}{3} \leq \omega t \leq \frac{5\pi}{3}$)	Sector VI ($\frac{5\pi}{3} \leq \omega t \leq 2\pi$)
$T_4 = \frac{\sqrt{3}}{2} m T_s \cos(\omega t + \frac{7\pi}{6})$	$T_5 = \frac{\sqrt{3}}{2} m T_s \cos(\omega t + \frac{5\pi}{6})$	$T_6 = \frac{\sqrt{3}}{2} m T_s \cos(\omega t + \frac{\pi}{2})$
$T_5 = \frac{\sqrt{3}}{2} m T_s \cos(\omega t + \frac{\pi}{2})$	$T_6 = \frac{\sqrt{3}}{2} m T_s \cos(\omega t + \frac{\pi}{6})$	$T_1 = \frac{\sqrt{3}}{2} m T_s \cos(\omega t + \frac{11\pi}{6})$
$T_0 + T_7 = T_s - T_4 - T_5$	$T_0 + T_7 = T_s - T_5 - T_6$	$T_0 + T_7 = T_s - T_1 - T_6$

In practice, however, the formulae in table 2.1 are seldom used directly. Most control algorithms work so, that the modulator receives the reference voltage vector. Therefore the cosine function has to be split using the well-known trigonometric identity $\cos(\alpha + \beta) = \cos(\alpha)\cos(\beta) - \sin(\alpha)\sin(\beta)$. Then the value of β can directly be determined from the sector the reference voltage vector is in and the value of $m \cos(\omega t)$ can be determined from the voltage vector itself. The sector the reference voltage vector is in can be determined by looking at the individual components of the said vector; for example if $u_a^* > u_b^* > u_c^*$ the vector is in sector I, while in sector II $u_b^* > u_a^* > u_c^*$ [4]. Alternatively it is possible to examine the state and voltage vectors and to exploit the fact that $\vec{S}_1 \times \vec{S}_1 = \vec{S}_2 \times \vec{S}_2 = 0$ and that $\vec{S}_1 \times \vec{S}_2 = -\vec{S}_2 \times \vec{S}_1 = \frac{\sqrt{3}}{2}$. Then equation 2.13, which represents the decomposition of \vec{U} in sector I, can be multiplied by \vec{S}_2 and \vec{S}_1 from the right side. This results in the following two relations

$$T_1 = \frac{3}{2} \frac{T_s}{V_{DC}} \frac{|\vec{V}_{ref} \times \vec{S}_2|}{|\vec{S}_1 \times \vec{S}_2|} = \sqrt{3} \frac{T_s}{V_{DC}} |\vec{V}_{ref} \times \vec{S}_2| \quad (2.14)$$

$$T_2 = \frac{3}{2} \frac{T_s}{V_{DC}} \frac{|\vec{V}_{ref} \times \vec{S}_1|}{|\vec{S}_2 \times \vec{S}_1|} = \sqrt{3} \frac{T_s}{V_{DC}} |\vec{V}_{ref} \times \vec{S}_1|. \quad (2.15)$$

The vectors $\vec{U}_1, \dots, \vec{U}_6$ are called the active vectors and the vectors \vec{U}_0 and \vec{U}_7 are called the zero vectors. It turns out that the sequencing of the active vectors is identical in all SVM modulators. The placement of the zero vectors differentiates different modulators from each other. A number of strategies for choosing the zero vector placement exist. [1]

Each of the carrier-based pulse-width modulation strategies can be converted into an SVM strategy. An example of the mapping of a carrier-based PWM to an SVM version in sector I is presented in figure 2.5. From this figure it is possible to deduce with the help of the equivalent volt-second principle the following relations,

$$U_{aN}T_s = \frac{V_{DC}}{2}(u_a^* + e_i)T_s = \frac{V_{DC}}{2}(T_1 + T_2 + T_7 - T_0) \quad (2.16)$$

$$U_{bN}T_s = \frac{V_{DC}}{2}(u_b^* + e_i)T_s = \frac{V_{DC}}{2}(T_2 + T_7 - T_0 - T_1) \quad (2.17)$$

$$U_{cN}T_s = \frac{V_{DC}}{2}(u_c^* + e_i)T_s = \frac{V_{DC}}{2}(-T_1 - T_2 + T_7 - T_0) \quad (2.18)$$

where $e_i(t)$ is the previously introduced zero sequence signal. From these relations it follows that the zero sequence signal determines the type of the modulator. Different functions $e_i(t)$ lead to different carrier-based PWM modulators. [4]

Unlike the previously introduced carrier-based PWM method, there are no separate modulation signals for the three phases in SVM and instead the voltage vector is processed as a whole. [6] This property makes SVM ideal for digital implementation. As microprocessors have developed, SVM has recently become one of the most important PWM methods for three-phase converters. It uses the space-vector concept to compute the duty cycles of the switches. Therefore, a space-vector modulator is simply the digital implementation of PWM modulators. [4] However, the main benefit of SVM is the explicit identification of pulse placement as an additional degree of freedom that can be exploited to achieve harmonic performance gains [1].

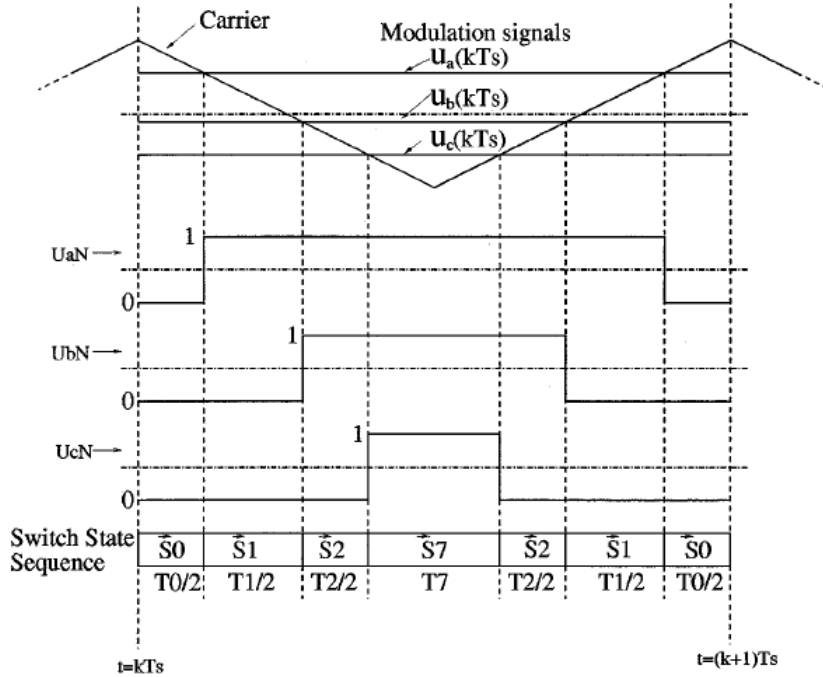


Figure 2.5: Representation of carrier-based PWM and how it maps to an SVM version of it [4].

2.1.3 Discontinuous pulse-width modulation

The fundamental difference between continuous PWM and discontinuous PWM reflects to the value of the zero-sequence component $e_i(t)$. For CPWM strategies in the linear range, $-1 - u_{min}^*(t) < e_i(t) < 1 - u_{max}^*(t)$, ($m \leq \frac{2}{\sqrt{3}}$), where $u_{min}^*(t)$ and $u_{max}^*(t)$ are the minimum and maximum of the modulation signal normalized to the range $[-1, 1]$. Therefore each output of the converter phase legs is switching between the positive or negative rail of the DC bus in each carrier signal period. However, for DPWM strategies the value of the zero-sequence component is $e_i(t) = -1 - u_{min}^*(t)$ or $e_i(t) = 1 - u_{max}^*(t)$. Thus the value of one modulation signal will be equal to ± 1 and the corresponding leg is tied to the positive or negative rail of the DC bus without switching actions. Alternatively this can be viewed as only one of the zero switching states being utilized per switching cycle. This makes it possible to reduce

the average switching frequency by 33 % and therefore cause less switching losses. [4]

A straightforward way to present the differences between various DPWM algorithms is to look at the space-vector placement and distribution. For the purposes of comparison, figure 2.6 presents this for a regular sampled PWM and for a regular sampled PWM with injected 3rd harmonic. A commonly used method to achieve discontinuous switching is to move the active space-vectors to eliminate one of the two zero space-vectors. Figures 2.7a and 2.7b present the DPWMMIN and DPWMMAX strategies. [1] In the case of DPWMMAX $e_i(t) = 1 - u_{max}^*(t)$ and its equivalent distribution of zero vectors is $T_0 = 0$ and $T_7 = T_s - T_1 - T_2$ in all six space-vector sectors. The case when $e_i(t) = -1 - u_{min}^*(t)$ is called DPWMMIN and its zero vector distribution is $T_7 = 0$ and $T_0 = T_s - T_1 - T_2$ in all six space-vector sectors. [4]

It is possible to further improve the discontinuous modulation strategy by alternating the zero space vectors \vec{S}_0 and \vec{S}_7 for successive 60° segments of the fundamental cycle. It has the benefit of symmetrical l-l voltages. This type of discontinuous switching pattern is called DPWM1 and it centers the nonswitching periods for each phase leg symmetrically around the positive and negative peaks of its fundamental reference voltage. This kind of placement is optimal for a resistive load, because there is no lag between the current and voltage vectors. Obviously, it is possible to place each 60° non-switching period anywhere within the 120° region where the appropriate phase leg reference voltage is at the maximum or minimum of the three-phase set. This gives rise to DPWM0, DPWM2 and DPWM3. In DPWM0 the non-switching period is advanced by a maximum 30° and in DPWM2 it is retarded by a maximum of 30° . However, this introduces asymmetry into the l-l voltage. [1] A Key difference is that DPWM1 is optimized for unity power factor loads, while DPWM0 is optimized for 30° leading power factor and DPWM2 is optimized for 30° lagging power factor loads. [3] Finally, it is also possible to clamp the phase legs to the opposite DC rails in each 60° segment. This gives rise to the DPWM3 switching strategy. [1] These four improved

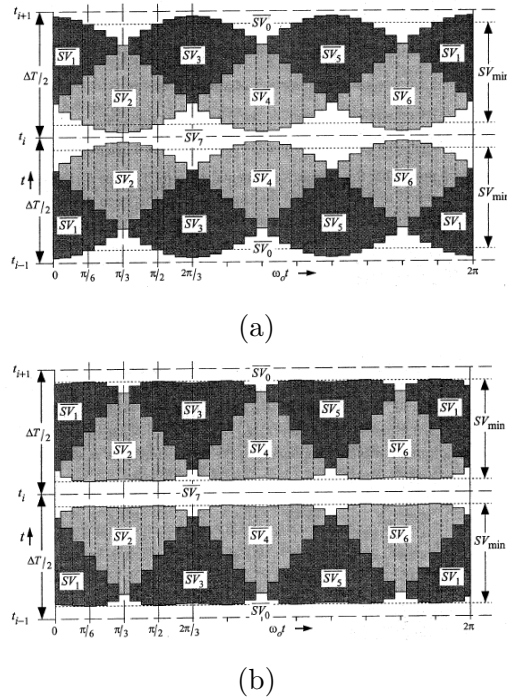


Figure 2.6: Figure 2.6a represents space-vector placement for a regular sampled PWM whereas 2.6b represents it for a regular sampled PWM with 3rd harmonic injected. The bars represent the distribution of the switching states. The width of the bars is off scale. [1]

DPWM strategies are shown in figure 2.7. In actual implementations these strategies are varied depending on the load and the measured currents. For instance, if the measured current vector was behind the commanded voltage-vector, the strategy for zero sequence placement could change to DPWM2 from whatever it was before.

2.1.4 Hysteresis based modulation

During the past decades a number of modulation strategies based on the hysteresis phenomenon have been developed. While these strategies differ drastically from one another they still heavily utilize the previously discussed state-vector concept. The main idea behind hysteresis based modulation

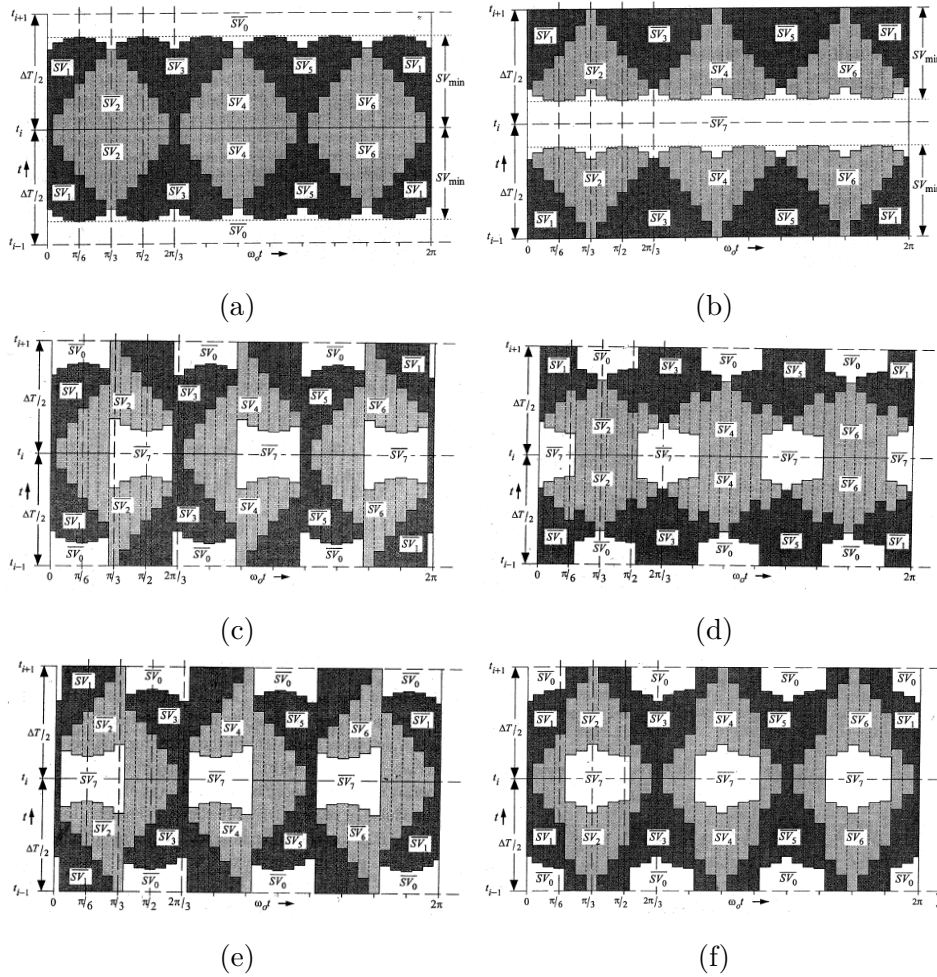


Figure 2.7: Figure 2.7a represents space-vector placement for DPWMMIN whereas 2.7b represents DPWMMAX. Figure 2.7c presents DPWM0 (30° leading clamp), Figure 2.7d presents DPWM1 (zero clamp at voltage peak), figure 2.7e presents DPWM2 (30° lagging clamp) and figure 2.7f presents DPWM3 (30° alternating clamp). The bars represent the distribution of the switching states. The width of the bars is off scale. [1]

strategies is to turn the switches in a way, which makes the controlled variables return back to their tolerable bands as fast as possible. Among these strategies the hysteresis band current control is used often due to the simplicity of its implementation. The basic implementation of hysteresis current

control (HCC) is based on deriving the switching signals from the comparison of the actual phase current with the tolerance band around the reference current [7]. Another example of a hysteresis based modulator is the direct torque control (DTC) modulator. In DTC the variables torque and flux are controlled using a hysteresis band.

The concepts introduced in the previous discussion about SVM can be applied also in hysteresis based modulation strategies. For example in 1998 B.-H. Kwon et al. presented an HCC strategy, which bases its logic on the measured inverter currents. Using the measured currents they detect the region the voltage vector currently is in and then the processed current measurements are used to select the correct switching states from a pre-calculated switching function table. The switching states presented in their method are the same ones utilized in SVM. [7] Because of these similarities, it is possible to optimize the switching process as earlier and thus reduce the switching losses by a major amount. It is clear, however, that due to the nature of the HCC algorithm it is difficult to derive analytic solution to its output. This makes analysing the harmonic response of such algorithms much more challenging. Additionally, the controller and the pulse generation part (modulator) of strategies of this kind are strongly interwoven.

The block diagram of a classical DTC implementation is presented in figure 2.8. The stator flux amplitude Ψ_{sc} and the electromagnetic torque M_{ec} are the reference signals, which are compared with their estimated values $\hat{\Psi}_s$ and \hat{M}_e . The flux and torque errors e_Ψ and e_M are delivered to the hysteresis controllers and the digitized output variables d_Ψ and d_M and the stator flux position sector $\gamma_{ss}(N)$ determine the appropriate voltage vector from the switching table. [8]

2.2 Harmonic analysis

One of the main differences between the various modulation methods are the harmonic frequencies they yield. This means, that the harmonics are char-

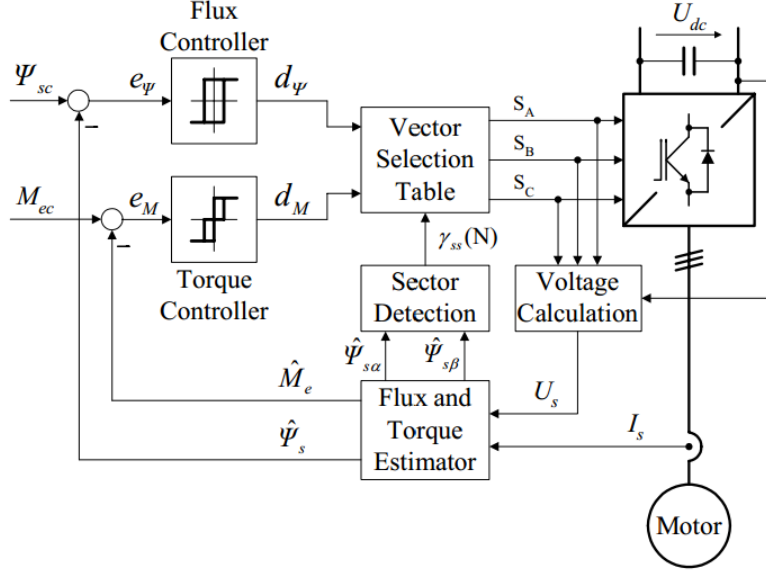


Figure 2.8: Block diagram of a classical DTC implementation [8].

acteristic to the modulation method. These have a great impact on power converter applications due to the need for electromagnetic (EM) shielding and filters. [1] While analytic analysis of the harmonics is relatively complicated, back in 1975 S. Bowes et al. developed a method, which adapted the theory originally developed for communication systems. This method is called the double integral analysis and is in essence based on Fourier series expansion in two variables. This is necessary since no rational relationship exists between the modulating frequency and the carrier frequency. This makes a single variable Fourier expansion inapplicable, since the waveform is not periodic. [9]

There are two variables assumed to exist in the double Fourier analysis. First define a time variable variable $x(t) = \omega_c t + \theta_c$, where $\omega_c = \frac{2\pi}{T_s}$ is the carrier angular frequency, θ_c is an arbitrary phase offset angle for the carrier waveform, and T_s is the carrier interval (or sampling interval). Then define a second time variable $y(t) = \omega_0 t + \theta_0$, where $\omega_0 = \frac{2\pi}{T_0}$ is the angular frequency of the fundamental waveform, θ_0 is an arbitrary phase offset angle for the

fundamental waveform, and T_0 is the wavelength of the fundamental waveform. These two variables $x(t)$ and $y(t)$ can be thought of as representing the time variation of the high-frequency modulating wave and low-frequency modulated wave. Each of the variables is considered independently periodic. Therefore, the problem of solving for the modulated $f(t)$ waveform can then be addressed by exploring the existence of a unit cell, which identifies contours within which $f(t)$ is constant for cyclic variations of $x(t)$ and $y(t)$. Such unit cell is presented in figure 2.9. [1]

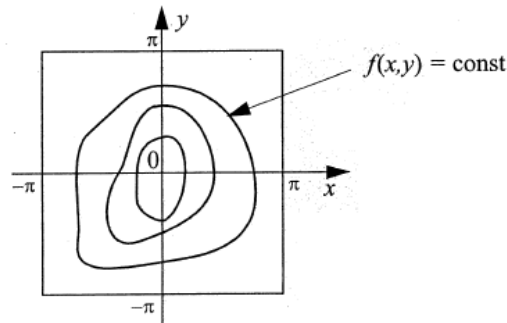


Figure 2.9: The unit cell which identifies contours within which $f(t)$ is constant for cycling variations of $x(t)$ and $y(t)$. [1]

The value of the function $f(t) = f[x(t), y(t)]$ within each contour region over the unit cell represents the output phase leg voltage. It simplifies the situation when this value is presented in three-dimensional form so that z-axis takes on the values of $f(x, y)$. The x-axis and y-axis of the cell are scaled in radians corresponding to the frequency of the modulating carrier and low-frequency reference waveforms. If it is assumed, that identical unit cells exist infinitely in both the x- and y- directions, it follows that Fourier expansion can be applied due to the periodicity. [1] The representation of the

series expansion given by Bowes is

$$\begin{aligned}
 f(x, y) = & \frac{A_{00}}{2} + \sum_{n=1}^{\infty} [A_{0n} \cos ny + B_{0n} \sin ny] \\
 & + \sum_{m=1}^{\infty} [A_{m0} \cos mx + B_{m0} \sin mx] \\
 & + \sum_{m=1}^{\infty} \sum_{\substack{n=-\infty \\ n \neq 0}}^{\infty} [A_{mn} \cos(mx + ny) + B_{mn} \sin(mx + ny)]
 \end{aligned} \tag{2.19}$$

where

$$A_{mn} + iB_{mn} = \frac{1}{2\pi^2} \int_0^{2\pi} \int_0^{2\pi} f(x, y) e^{i(mx+ny)} dx dy. \tag{2.20}$$

It is useful to note, that the terms of equation 2.19 have specific physical meanings. The first term is the DC-offset. The second summation term contains the fundamental component and baseband harmonics. This term includes low-order undesirable harmonics around the fundamental output which should be minimized. The third summation term contains the carrier harmonics, which are generally very high-frequency components, because the lowest frequency term is the modulating carrier frequency. The final double summation contains side band harmonics, which contain all the possible frequencies formed by taking the sum difference between the modulating carrier waveform harmonics and the reference waveform and its associated harmonics. These components tend to exist as groups around the carrier harmonic frequencies. It can be shown, for example, that for the case of naturally sampled triangular carrier PWM, which was shown in figure 2.1, the voltage has the following Fourier expansion

$$\begin{aligned}
 v_{an}(t) = & \frac{V_{DC}}{2} M \cos(\omega_0 t + \theta_0) \\
 & + \frac{2V_{DC}}{\pi} \sum_{m=1}^{\infty} \frac{1}{m} J_0 \left(m \frac{\pi}{2} M \right) \sin m \frac{\pi}{2} \cos(m[\omega_c t + \theta_c]) \\
 & + \frac{2V_{DC}}{\pi} \sum_{m=1}^{\infty} \sum_{\substack{n=-\infty \\ n \neq 0}}^{\infty} \frac{1}{m} J_n \left(m \frac{\pi}{2} M \right) \sin \left([m + n] \frac{\pi}{2} \right) \\
 & \times \cos(m[\omega_c t + \theta_c] + n[\omega_0 t + \theta_0])
 \end{aligned} \tag{2.21}$$

where J_n is Bessel function of the first kind. [1]

While possible, application of double Fourier analysis to SVM is no longer trivial, because the reference waveform is not continuous but it is made up of six segments across a complete fundamental cycle. Hence the outer integral term becomes a summation of six integral terms, each spanning 60° of the fundamental. As a result the equation defining the coefficients of the series becomes

$$A_{mn} + iB_{mn} = \frac{1}{2\pi^2} \sum_{m=1}^6 \int_{y_s(i)}^{y_e(i)} \int_{x_r(i)}^{x_f(i)} V_{DC} e^{i(mx+ny)} dx dy \quad (2.22)$$

where $x_r(i)$ is the rising edge of switched waveform, $x_f(i)$ is the falling edge of switched waveform. [1]

This analytic method only applies to the modulation strategies where the signals are periodic. As a result, it is not possible to apply double Fourier analysis to strategies fully based on hysteresis. This is due to the stochastic nature of these modulation strategies. The mostly used strategy for defining the harmonic behaviour in these cases is numerical simulation or physical measurement using standard measurement tools. The spectrum of the hysteresis based modulation strategies generally lacks distinct harmonics and, apart from the fundamental peak, is generally flat noise.

2.3 Minimum pulse-width limitations

The concept of minimum pulse-width (MPW) limitations is closely related to the concept of dead time. The dead time means the intentional delay introduced into switching in order to prevent a shoot-through condition, where both of the semiconducting switches of a power pole are conducting at the same time. In order to prevent this situation, a delay has to be introduced to the switching of the complementary switches in any of the three power poles. If the switches were ideal and therefore fully complementary, such delay would not be required. [1]

The MPW limitations arise from the fact that the shortest possible realizable pulse in the used modulation strategy in a specific power conversion system is not arbitrarily short. The limitations result when small on time duration of the lower switch in a phase leg cannot be achieved. Since the upper switch in the phase leg is gated in a complementary manner, maximum achievable pulse duration is effectively induced. The complementary is also true if the upper switch is limited to a maximum on-time duration, introducing an effective minimum pulse width on the lower switch. Such limitations are enforced to prevent damage to the power converter and the surrounding circuitry. Additionally the constraints set by the power converter topology, such as the parameters of the gate driver, also cause MPW limitations. [3]

The connection to dead-time is introduced, when the inverter PWM voltage approaches its maximum value. In this situation the width of the pulses becomes increasingly narrow. When any pulse width is reduced to the dead-time, it cannot be decreased further. This process is termed *lockout*. [1] Traditionally, pulses less than a minimum width were prevented from passing to the gate driver circuit and hence dropped. However, this dropping of pulses results in the rounding of the phase duty cycle. [3] This process is termed *dropout* [1]. Another approach is to hold pulses which are too small to be achievable to the minimum achievable pulse-width. A hybrid approach is also possible: pulses are dropped if they are very small, but held to the minimum pulse-width value if only slightly smaller. These three approaches and their effect to the duty cycle is presented in figure 2.10. [3]

Because each of the three possible ways of handling pulses shorter than the minimum width causes clamping of the desired duty cycle to a certain level, it is obvious that this affects the performance of the power converter. For instance, distorting the output signal by clamping the duty cycle to a certain level introduces more unwanted harmonics to the output of the converter. The linear modulation range is also reduced due to the larger distortion [3]. Because the modern digital systems are capable of implementing any of the three minimum pulse-width handling methods, this thesis focuses on the third

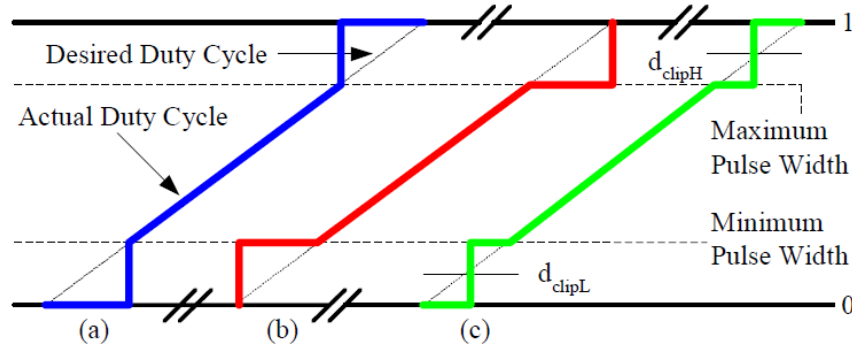


Figure 2.10: There are three possible ways of handling pulses shorter than the minimum width. In (a) the pulses are dropped resulting in the rounding of the phase duty cycle. In (b) the pulses are held to the minimum achievable pulse-width and in (c) the pulses are dropped if they are very small, but held to the minimum pulse-width value if only slightly smaller. [3].

method. The third method is by far the most useful for industry applications, because it balances the lost and gained volt-seconds.

In practice the limitations directly affect the maximum and minimum duty cycles of the device. The effect on duty cycle is determined by both the dead-time and the MPW limitations, because in order to produce pulses, which are correctly limited by the MPW limitations, one must include the effect of dead-time. Figure 2.11 presents how the dead-time is introduced to switching by ensuring the two switches of a power pole never conduct at the same time. The resulting minimum and maximum duty cycles can be derived from the figure and are by B. Welchko et al. suggested to be

$$d_{max} = 1 - (1/T_s)(2T_{dead} + T_{MPW}) \quad (2.23)$$

$$d_{min} = (1/T_s)(2T_{dead} + T_{MPW}). \quad (2.24)$$

However, because the dead-time compensation occurs after the PWM modulator signal, different limits on duty cycle for the modulator are induced. In effect, this further shifts the duty cycle limits towards the center, $d = 0.5$ by one dead-time period. Therefore, the practical limits on duty cycle at the

output of the PWM modulator are given as

$$d_{max} = 1 - (1/T_s)(3T_{dead} + T_{MPW}) \quad (2.25)$$

$$d_{min} = (1/T_s)(3T_{dead} + T_{MPW}) \cdot [3] \quad (2.26)$$

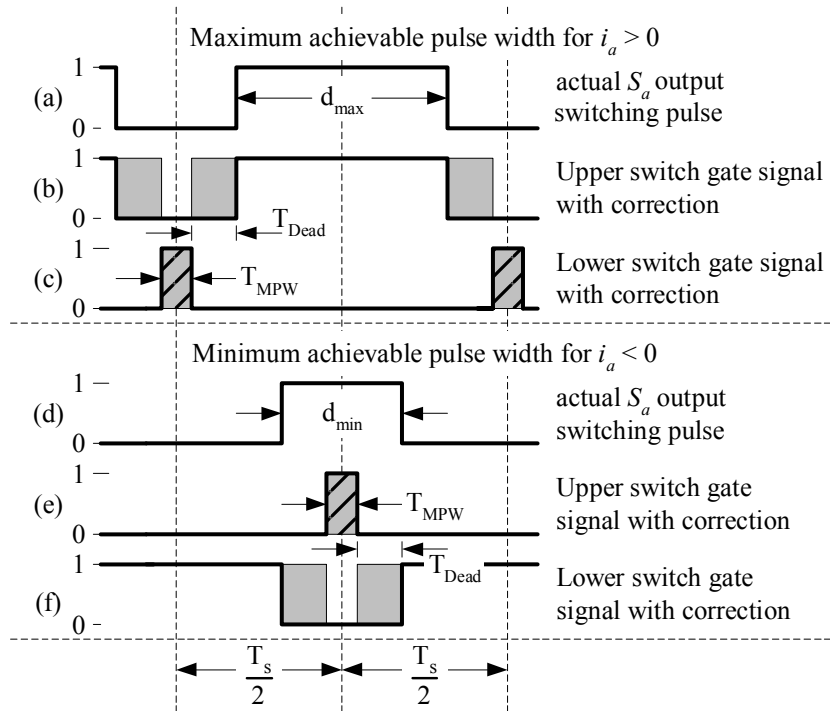


Figure 2.11: Gate signals for the maximum and minimum achievable pulse widths [3].

Chapter 3

Physical constraints

While in chapter 2 the theory behind ideal modulation was discussed, in reality the physical components of the power converter are not ideal. As a result, their effect on the MPW limitations has to be taken in account. In this chapter the components affecting the limitations are identified and their effect is discussed. The fact that the components are not ideal makes it difficult to determine the actual width of the shortest achievable pulse.

The components are divided into three categories. First the components of the inverter output bridge are identified and analysed. Then the DC bus (also known as the DC circuit) of the power converter is examined. Third the effect of the cable connecting the load to the power converter is looked at. Each of the components contributes to the MPW limitations and the one providing the maximum effect determines the actual limitations required for the application.

3.1 Inverter output bridge components

The structure of a 3-phase voltage source inverter was presented in figure 1.1. The inverter output bridge is the part of the inverter, which consist of the switching semiconductors, free-wheeling diodes and the gate drivers controlling the switches. These components place the fundamental limit to

the minimum pulse width by defining the dead time required by the converter.

3.1.1 Switching semiconductors

Semiconducting components used as switches is the most common method of modulating the output signal of a power converter. Commonly the components used for this purpose are gate turn-off thyristors (GTO) and its successor integrated gate-commutated thyristor (IGCT), insulated-gate bipolar transistors (IGBT) and metal-oxide-semiconductor field-effect transistors (MOSFET). The choice of the switching component depends on the application. While GTOs can withstand the highest currents and voltage differences across the device, they cannot be switched on and off very fast. On the other hand IGBTs can handle switching frequencies up to tens of kilohertz but their voltage and current tolerances are considerably lower than those of GTOs. The fastest switching frequencies can be obtained using MOSFETs, however, their rated voltage and current tolerances are even lower than those of IGBTs. Figure 3.1 depicts the different application domains of the switches. [2, 10]

Normal thyristors are not fully controllable switches as they cannot be turned off. The GTO can be turned on by applying a current pulse of positive polarity on the gate and turned off by a current pulse of negative polarity. Like the standard thyristor, the GTO is a four layer device with three junctions. The layers are p-n-p-n, where the outer p-layer provides anode connection, and the outer n-layer provides the cathode connection. In order to achieve high emitter efficiency, the cathode layer is generally highly doped to n+. However, this causes the junction nearest to the cathode have a low breakdown voltage. The structure of a GTO is shown in figure 3.2. [11]

The GTO operates very similarly to a standard thyristor and it can thus be thought of being one PNP and one NPN transistor being connected in a regenerative configuration. This means that the system maintains itself in the state once it has been turned on. No current will flow once a potential is applied across the GTO and this mode is called the forward blocking mode. To turn on the device it is necessary to inject charge carries into the

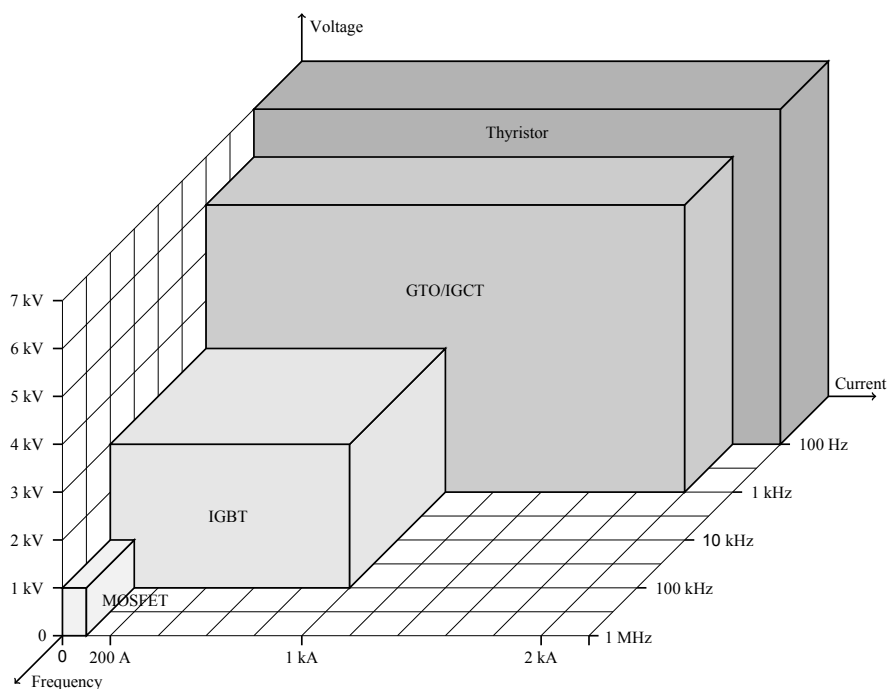


Figure 3.1: Different semiconductor switches have different application domains. Thyristors work only at low frequencies whereas IGBT and MOSFETs can operate at much higher frequencies. On the other hand, thyristors can withstand the highest currents and voltages. Figure reproduced from [2].

gate of the device. Alternatively the anode voltage can be risen until the avalanche multiplication process occurs. The latter, however, is generally not the desired way of using the component. In order to turn off a conducting GTO, the gate terminal is biased negative with respect to the cathode. The holes injected from the anode are then extracted through the gate. The resulting voltage drop causes reverse bias on the lower junction effectively stopping the current flow and turning off the device. The anode current does not stop instantly, but is collected into high density filaments in the most remote areas of the gate contact. These extremely localized high temperature regions can cause device failures unless they quickly dissipate. The GTO requires external snubber circuits to shape the turn on and off currents to prevent device destruction caused by too large current transients. [11]

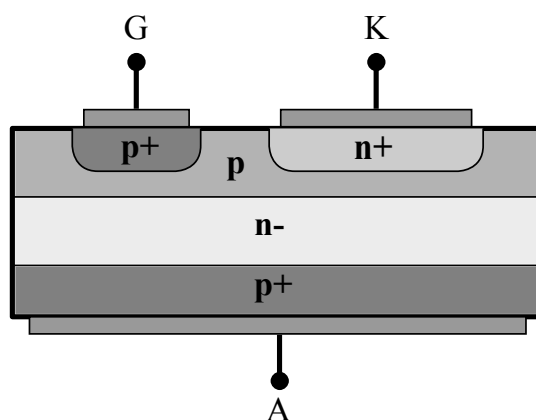


Figure 3.2: The cross-section of a GTO shows how it consists of p-n-p-n layers exactly like a normal thyristor. The major difference being the p+ region connecting the gate to the upper p -layer.

An IGCT, developed jointly by the companies ABB and Mitsubishi, is a direct improvement on the GTO. While the structure of the two devices is almost identical, an IGCT can be turned on and off much faster than a GTO. The reason for this is, that in an IGCT the gate turn off current is greater than the anode current resulting in a total elimination of minority carrier injection from the lower pn -junction. Due to this very high current no conventional wiring can be used and the driving circuit must be directly connected to the semiconductor using a printed circuit board (PCB). [12]

While not suitable for very high power applications due to its on state resistance, MOSFETs are capable of unmatched switching frequency and they are simple to control. The operation of a MOSFET is based on the modulation of charge concentration by a MOS capacitance between the body and gate electrodes of the device. The device consists of a semiconducting substrate, which is coated with a thin layer of insulating oxide. On top of the oxide there is a conducting gate electrode (G). In modern power MOSFETs the gate is generally buried in a trench etched to the silicon wafer. The former design is called D-MOSFET and the latter U-MOSFET. On both sides of the gate the substrate has been strongly doped. These areas are

called source (S) and drain (D). The opposite doped area between source and drain is called the channel. The structure of a D-MOSFET and a U-MOSFET device is presented in figure 3.3. The region connecting the drain to the channel is called the drift region. The length of the drift region is a major factor in determining the off-state voltage capability of the device. However, long drift regions result in higher on-state resistance, thus inducing larger power losses. [10] It should be noted, that there is a number of different power MOSFET designs, and the D-MOSFET and U-MOSFET designs only account to a coarse, high-level classification.

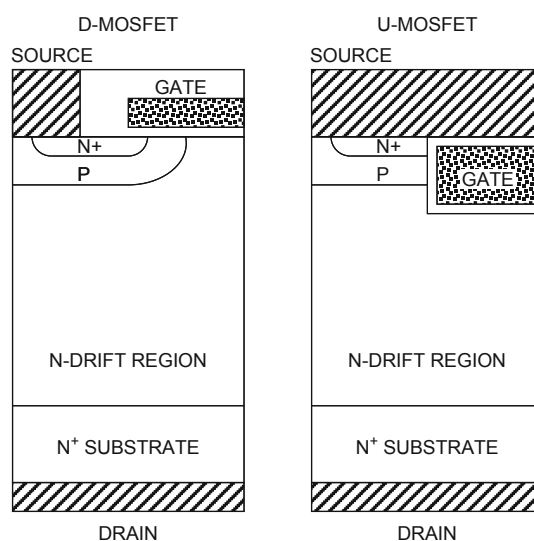


Figure 3.3: In the early power MOSFET designs (D-MOSFET) the gate electrode was located on the surface. In the modern MOSFET designs (U-MOSFET) the gate electrode is buried in a trench etched to the silicon wafer. [10]

Once voltage is applied across the device, the electric field passes through the channel. This induces an inversion channel, which for conduction has to be of the same type (p or n) as the drain and the source. The current will pass through this channel. The conductivity of the inversion channel may be modified by altering the voltage difference between the gate and the source or by altering the drain current. If the drain and the source are of n-type, positive gate-source voltage induces an n-channel allowing conduction.

The inverse is true for the drain and source of p-type: negative gate-source voltage induces a p-channel allowing conduction. [10]

The IGBT combines the simple gate-drive characteristics of MOSFETs with the high current capabilities of bipolar transistors. The IGBT combines an isolated FET for controlling the input and a bipolar transistor acting as the actual switch. An IGBT is similar in construct to an n-channel power MOSFET with one crucial difference: the n⁺-drain is replaced with a p⁺-collector layer. This forms a vertical PNP bipolar transistor inside the device. As the blocking voltage rating of semiconducting devices increases, the depth of the drift region must increase and the doping must decrease. This results in an approximately square relationship decrease in forward conduction versus the capability of blocking voltage. In IGBT, minority charge carriers are injected from the collector p⁺-region into the drift region during forward conduction. This considerably decreases the on-state resistance and the forward voltage drop of the device. This allows for a longer drift region making it ideal for high power applications. However, the additional pn-junction blocks reverse current flow, making it impossible for IGBTs to ever conduct in reverse direction. Due to this property, a diode is always connected in parallel with an IGBT. The structure of an IGBT is presented in figure 3.4. [13]

Each of these devices has their own field of application in modern power converters. The devices have drastically different switching characteristics in terms of speed and recovery time. This means, that the dead time and, thus, the minimum pulse width requirements are fundamentally affected by the type of the semiconducting switch.

Fast GTO thyristors have a recovery time of several tens of microseconds. Most of the charge carriers responsible for conduction in a thyristor leave the component as reverse current during turn off. However, as the current through the component decreases a cloud of charge carriers is trapped around the middle junction, because it is not in the vicinity of the depletion regions near the cathode and anode. These charge carriers can only

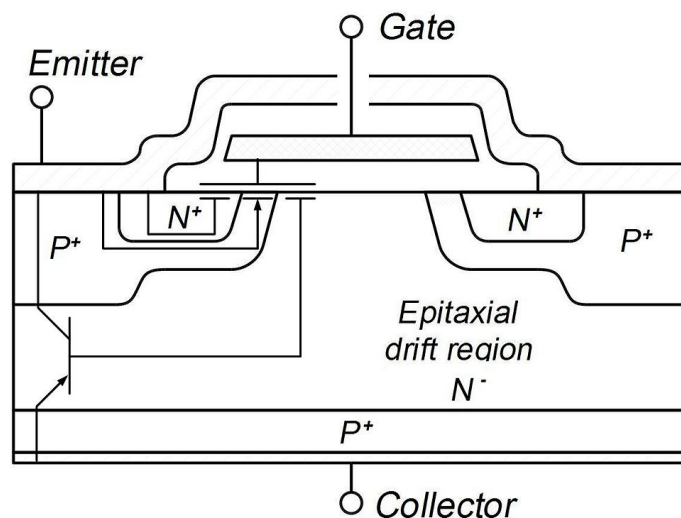


Figure 3.4: The IGBT device is similar to an n-channel power MOSFET. The n+ drain is replaced by a p+ collector. This renders a PNP bipolar transistor inside the device, which noticeably decreases the on-state resistance of the device.

be removed through recombination, which is slow due to the low dopant concentration. [14]

The MOSFET and the IGBT, due to the input MOS gate structure, are much easier to control as they do not need a current based pulse to the gate. However, IGBT switching times are longer, because the charge carriers in the lowermost pn -junction of the device must first be removed. The switching times of both devices are still considerably faster than those of GTOs and IGCTs.

3.1.2 Free-wheeling diodes

Power converters are often used to drive high inductance loads, such as electric motors. Due to this, there are strong reverse current transients when the semiconducting switches are turned off. Free-wheeling diodes connected in parallel with the switches protect the semiconducting devices from these inductive surges. Free-wheeling diodes are visible in figure 1.1 in parallel

with the switches.

The diodes have a fundamental characteristic causing major losses in the power converters. When the diode is switched from its conducting state to the non-conducting state by reversing the polarity of the voltage across it, the diode does not stop conducting instantly. Instead, the charge-carriers within the device must first flow out. This results in a characteristic of diodes called the reverse recovery time. The reverse recovery time can be of the order of several microseconds for fast high power diodes. [14]

While the reverse recovery time does not directly affect the minimum pulse-width limitations, because it is negligible in comparison to the other effects of the physical components, it has an indirect effect. The reverse recovery time affects the dead time of the power pole and thus changes the maximum and minimum duty cycle limitations of the system. As discussed in chapter 2 the minimum and maximum duty cycle limitations are related to both the dead time and the MPW limitations by equations 2.25 and 2.26. The reverse recovery time also limits the switching frequency the system is capable of, because the reverse recovery time results in switching losses, which are proportional to the switching frequency.

It is possible to practically eliminate the reverse recovery time by using silicon carbide Schottky diodes instead of the typically used silicon based P-i-N diodes [10]. Because the conductivity of Schottky diodes is based on the movement of majority charge carriers only, they have no recovery time. Therefore, in theory, they have no reverse recovery current. In practice, however, the internal capacitance of the component results in a recovery time of the order of hundred nanoseconds. [14]

The structure of a power MOSFET was shown in figure 3.3. It is worth noting that there is always an integrated diode inside a MOSFET. Therefore, in theory, MOSFET devices do not necessarily need an external free-wheeling diode parallel to them. However, in practice, the device structure is not always optimized for the performance of the integrated diode. [10] Therefore free-wheeling diodes are commonly seen in parallel with MOSFETs as well.

3.1.3 Gate driver limitations

Gate driver is the circuit applying the required voltage or current pulse to the gate (or any other controlling structure) of the semiconducting device in order to turn it on and off. The gate driver circuit is completely based on the type of the semiconductor. For example the circuit to drive thyristors is completely different from the circuit driving IGBTs.

The gate driver of a GTO thyristor must be able to produce both negative and positive current pulses. If the GTO is switched off rapidly, the reverse gate current must be of the same magnitude as the anode current to be extinguished. This requirements often forces the designers to use expensive components, such as inductors. [15] The complexity of the gate drive circuit for GTOs makes it slower in operation. Thus, it provides reduced switching frequencies.

Both power MOSFETs and IGBTs are voltage-controlled devices and have a very high input impedance. To turn on a MOSFET or an IGBT, only a small amount of charge is required to be injected into the gate and build up a gate voltage higher than the turn-on threshold voltage. During the on-state, the gate only draws a small leakage current of the order of nano amperes. Due to this, the gate driver circuit for MOSFETs and IGBTs is much simpler than that for thyristors. [16]

The capability of the gate driver to generate the pulse controlling the semiconducting device directly affects the minimum pulse-width requirements. If the controlling circuit is not capable of turning device on and off in rapid enough succession, the minimum pulse-width must be limited along with the used switching frequency. In the case of modern gate drivers it is possible to switch an IGBT module rated at 800A/3300V up to 3000A at 2200V in $3 \mu s$ [17].

3.2 DC circuit oscillations

The energy that flows through a power converter must be stored so that the switches can convey the correct amount of it to the load. Generally, a capacitor array is used for this purpose and the circuit storing the energy is called the DC circuit. The DC-capacitors store the energy, which is transmitted to the load.

The capacitance of the DC-capacitor array and the natural inductance and resistance of the system result in a damped oscillator. Therefore, the modulation process induces unwanted oscillations to the DC circuit. Additionally the harmonics caused by the modulation process and the load can also pass through to the DC circuit, causing further oscillations.

If the capacitors are large enough, the modulation process does not cause major fluctuations in the DC circuit voltage. However, sometimes the commonly used electrolytic capacitors are replaced with more reliable and robust film capacitors. This results in a major drop of capacitance resulting in a poorly damped DC circuit. [18] It is, thus, suggested by K. Pietiläinen et al. that power converters equipped with such film capacitors require active stabilization using a control system they describe [19].

As the power flow through the power converter increases, the power density of the converter does not increase as rapidly. Therefore, the physical size of power converters increases as the power requirements increase. Additionally this results in physically larger power conveying components, such as DC bus bars. The increased size results in increased resistance and inductance, which amplifies the DC oscillatory behaviour of the DC circuit [20].

As stated earlier, the effect of modulation on the DC bus voltage measured from the terminals of the capacitor array can be small for large capacitors. However, when measured from the terminals of the switching semiconductors there can be much larger voltage fluctuations. This results from the inductance of the DC bus bars and the capacitance of the clamp capacitors. Often snubber capacitors are added close to the switching semiconductor to

eliminate these voltage spikes. However, careful design of the bus bars can dramatically reduce the voltage spikes around IGBT terminals. [20] This effect has to be considered in MPW limitations. If the distance between PWM pulses is too short and switching causes constant over voltage spikes at the terminals of the IGBT, the life time of the device can be expected to decrease.

Physically the phenomenon is easy to understand, when one considers the oscillating charge in the DC bus bars. If the next switching event on the semiconductor side happens before the oscillating charge caused by the previous switching event has decayed, there happens cumulation, which can result in large voltage spikes. Therefore, it is important to define the MPW limits so, that there is enough time for the decay process.

The exact effect of DC circuit oscillations on the MPW limitations is difficult to determine quantitatively, because the oscillations are directly determined by the implementation. While in some systems the effect of the oscillations is negligible, in others the effect may be the determining factor for the final MPW limits. Thus, the limitations should be considered separately for the power converter in question and not universally.

3.3 Cable oscillations

The increase in switching frequency due to faster semiconductors (MOSFET and IGBT) has led to decreased harmonics and shrinking of the filters attached to the power converter, which has increased the efficiency of power converters. The acoustic noise has also decreased. However, in addition to the benefits, the increased switching frequency also results in a new phenomenon causing a current oscillation to the start of the cable connecting the power converter to the load and a voltage oscillation to the end. [21] This effect is traditionally eliminated using relatively expensive output signal filters.

A transmission line is a specialized cable or other structure, which takes in account the wave nature of the travelling signal. While the switching fre-

quency of power converters is not extremely high, the pulse length is often so short that the cable connecting the converter to the load should be considered a transmission line. Transmission lines induce oscillatory phenomena to the power converter, which originate from the reflection of the travelling pulse from an impedance mismatch. The motivation for studying cable oscillations originates from the possibility of voltage spikes several times larger than the DC circuit voltage. [22]

3.3.1 Oscillation of the reflected wave

A transmission line can be reduced to a set of differential equations, the so called telegrapher's equations.

$$\frac{\partial}{\partial x}u(t, x) = -ri(t, x) - l\frac{\partial}{\partial t}i(t, x) \quad (3.1)$$

$$\frac{\partial}{\partial x}i(t, x) = -gu(t, x) - c\frac{\partial}{\partial t}u(t, x) \quad (3.2)$$

These equations can be derived from figure 3.5, which represents a differential slice of the transmission line. Therefore, x represents a point along the transmission line and r , l , g and c are the distributed resistance, inductance, conductance and capacitance. In the differential slice, the distributed parameters are considered equally distributed and thus independent from parameter x .

Through Laplace transform the equations 3.1 and 3.2 reduce to

$$\frac{d}{dx}U(s, x) = -(r + sl)I(s, x) \quad (3.3)$$

$$\frac{d}{dx}I(s, x) = -(g + sc)U(s, x). \quad (3.4)$$

These equations can be further Laplace transformed using the initial conditions $U(s, x = 0) = U(s, 0)$ and $I(s, x = 0) = I(s, 0)$ yielding

$$pU(s, p) - U(s, 0) + (r + sl)I(s, p) = 0 \quad (3.5)$$

$$pI(s, p) - I(s, 0) + (g + sc)U(s, p) = 0. \quad (3.6)$$

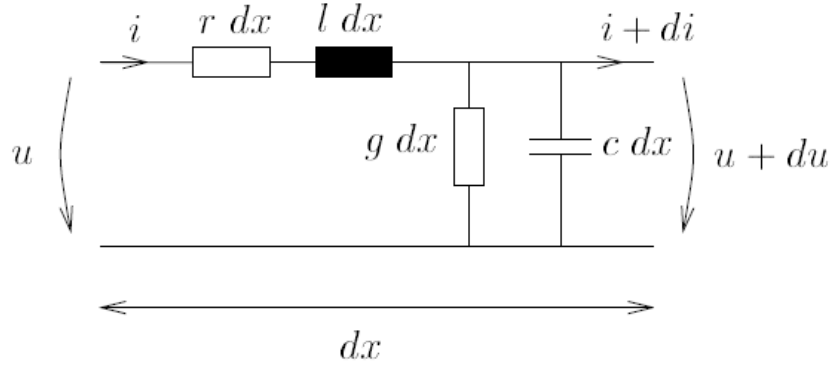


Figure 3.5: Differential slice of a transmission line. The figure contains the distributed resistance (r), the distributed inductance (l), the distributed conductance (g) and the distributed capacitance (c). [21]

Now it is possible to solve for $U(s, p)$ and $I(s, p)$ resulting

$$U(s, p) = \frac{pU(s, 0) - (r + sl)I(s, 0)}{p^2 - (g + sc)(r + sl)} \quad (3.7)$$

$$I(s, p) = \frac{pI(s, 0) - (g + sc)U(s, 0)}{p^2 - (g + sc)(r + sl)}. \quad (3.8)$$

Defining the variables

$$Z_c = \sqrt{\frac{sl + r}{sc + g}} \quad (3.9)$$

$$\gamma = \sqrt{(sl + r)(sc + g)}, \quad (3.10)$$

where Z_c is the characteristic impedance of the cable and γ is the propagation constant, lets equations 3.7 and 3.8 take the form

$$U(s, p) = \frac{pU(s, 0) - \gamma Z_c I(s, 0)}{p^2 - \gamma^2} \quad (3.11)$$

$$I(s, p) = \frac{pI(s, 0) - \gamma/Z_c U(s, 0)}{p^2 - \gamma^2}. \quad (3.12)$$

Finally inverse Laplace transform yields

$$\begin{pmatrix} U(s, x) \\ I(s, x) \end{pmatrix} = \begin{pmatrix} \cosh(\gamma x) & Z_c \sinh(\gamma x) \\ \sinh(\gamma x)/Z_c & \cosh(\gamma x) \end{pmatrix} \begin{pmatrix} U(s, 0) \\ I(s, 0) \end{pmatrix}. \quad (3.13)$$

Assuming the wave only travels to the positive direction ($e^{\gamma x} = 0$) and by dividing the propagation constant γ to its real and imaginary parts α and β , the previous matrix representation reduces to

$$U(s, x) = U(s, 0)e^{-\alpha x} e^{i\beta x} \quad (3.14)$$

$$I(s, x) = I(s, 0)e^{-\alpha x} e^{i\beta x}. \quad (3.15)$$

The real part of the propagation constant is called the attenuation constant and the imaginary part is called the wave number. [21]

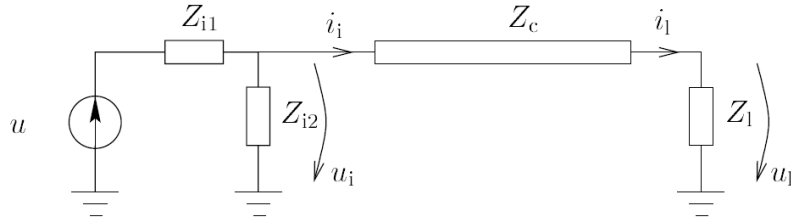


Figure 3.6: Circuit diagram of the power converter, load and the connecting cable. [21]

Unless the impedance of the load, power converter and the connecting cable have been matched, there is a change in characteristic impedance, when the signal changes medium. The circuit diagram of this system is presented in figure 3.6. Using the reflection and transmission coefficients

$$\rho = \frac{Z_b - Z_a}{Z_b + Z_a} \quad (3.16)$$

$$\tau = \frac{2Z_b}{Z_b + Z_a}, \quad (3.17)$$

where Z_a is the characteristic impedance of the first medium and Z_b that of the second medium, it is possible to derive transmission functions for the power converter, load and the connecting cable. Tarkiainen [21] gives the

result

$$\frac{U_l(s)}{U}(s) = \frac{e^{-\gamma(s)x}(1 + \rho_l(s))}{1 - \rho_l(s)\rho_i(s)e^{-2\gamma(s)x}} G(s) \quad (3.18)$$

$$\frac{U_i(s)}{U}(s) = \left(\frac{\rho_l(s)e^{-2\gamma(s)x}(1 + \rho_i(s))}{1 - \rho_l(s)\rho_i(s)e^{-2\gamma(s)x}} + 1 \right) G(s) \quad (3.19)$$

$$\frac{I_l(s)}{U}(s) = \frac{e^{-\gamma(s)x}(1 - \rho_l(s))}{1 - \rho_l(s)\rho_i(s)e^{-2\gamma(s)x}} \frac{G(s)}{Z_c(s)} \quad (3.20)$$

$$\frac{I_i(s)}{U}(s) = \left(\frac{-\rho_l(s)e^{-2\gamma(s)x}(1 - \rho_i(s))}{1 - \rho_l(s)\rho_i(s)e^{-2\gamma(s)x}} + 1 \right) \frac{G(s)}{Z_c(s)}, \quad (3.21)$$

where

$$G(s) = \frac{Z_c(s)Z_{i2}(s)}{Z_c(s)Z_{i2}(s) + Z_{i1}(s)(Z_c(s) + Z_{i2}(s))} \quad (3.22)$$

$$\rho_l(s) = \frac{Z_l(s) - Z_c(s)}{Z_l(s) + Z_c(s)} \quad (3.23)$$

$$\rho_i(s) = \frac{\frac{Z_{i1}(s)Z_{i2}(s)}{Z_{i1}(s)+Z_{i2}(s)} - Z_c(s)}{\frac{Z_{i1}(s)Z_{i2}(s)}{Z_{i1}(s)+Z_{i2}(s)} + Z_c(s)}. \quad (3.24)$$

Generally the loads connected to power converters are time variant, which means that at least one of the parameters of the load varies as a function of time. For instance, in an induction motor, the electric angular frequency varies. Because of this, the load impedance cannot directly be modelled as an impedance in Laplace space. Due to this, Tarkiainen suggests to combine the low and high frequency responses of a simplified RLC-load model. [21]

Currently many power converter applications accept the fact that cable oscillations cause voltage spikes. Thus the cable length for the applications is limited and the voltage rise time of the switches is controlled to keep the voltage spikes within acceptable limits. A model developed by S. Amarir et al. is closely related to the reflection analysis described above. Their model gives accurate results for the behaviour of the voltage in the cable connecting the load to the power converter. [23]

3.3.2 Pulse-width and cable oscillations

The previously discussed transmission line analysis explains voltage transients of less than two times the DC-bus voltage (< 2 -pu). However, certain PWM modulation cycles can lead to situations, where > 2 -pu voltage pulses are possible. For instance, if the last cable transient has not fully decayed before the application of the next pulse, the residual trapped charge may cause a 3-pu over voltage condition. [22] Therefore, pulse-width limitations must be applied to limit the pulse-width so, that there is always enough time for the last cable transient to decay.

It is important to have the reflected wave over voltage transient oscillation decay to zero before the arrival of the next PWM pulse. Therefore, the pulse-width limitations caused by cable oscillations are directly determined by this decay time. The determination of the decay time, however, is not exactly trivial due to a large number of parameters affecting it. A model for calculating the decay time, taking in account characteristic impedance, skin and proximity effects was developed by R. Kerkman et al. suggesting that the time to damp pulses to $< 5\%$ of their original amplitude is estimated by three times the time constant τ of

$$\frac{U}{U_0} = e^{-r_s x / 2Z_0} = e^{-r_s vt / 2Z_0} = e^{-t/\tau}, \quad (3.25)$$

where r_s (ac Ω /conductor/m) is the ac-resistance, Z_0 is the characteristic impedance and v is the velocity of the traversing wave. The ac-resistance of the cable is dependent on cable oscillation frequency and is increased above the DC value due to skin and proximity effects. Skin effect is due to the fact that the internal inductance of a conductor is highest at the center and lowest at the edges. The proximity effect is due to the magnetic fields of neighbouring adjacent conductors. The value of r_s is

$$r_s = K_p K_{skin(f_0)} R_{DC} = K_p \left(\frac{d_0}{2\delta} \right) \left(\frac{4\rho}{\pi d_0^2} \right) = \frac{2K_p \rho}{\pi \delta d_0}, \quad (3.26)$$

where K_p is the proximity effect increase ($K_p = 2$ for tightly bundled round conductor cables), $K_{skin(f_0)}$ is the skin effect factor at cable oscillation fre-

quency f_0 , R_{DC} is the DC resistance of the conductor, d_0 is the diameter of the conductor, ρ is the resistivity of the conductor and δ is the skin depth. [22] The skin depth can be approximated by $\delta = \sqrt{\frac{2}{\sigma\mu\omega}} = \sqrt{\frac{1}{\pi\sigma\mu f_0}}$, where μ and σ are the permeability and conductivity of the conductor metal respectively and ω is the angular frequency of the oscillation [24]. The skin depth is dependant on cable oscillation frequency, which can be calculated by using the equation

$$f_0 = \frac{1}{T_{cycle}} = \frac{1}{4t_p} = \frac{v}{4a} = \frac{1}{4a\sqrt{L_0C_0}}, \quad (3.27)$$

where a is the length of the cable, t_0 the time is traverse time of the wave, and L_0 and C_0 are the cable inductance and capacitance per unit length and they determine the wave velocity v and the characteristic impedance Z_0 of the cable [22].

Based on equation 3.25 the off time between pulses in order to prevent greater than 2-pu voltage transients turns out to be $T = 3\tau = \frac{6Z_0}{r_s v}$. This can be further simplified by acknowledging the relations $v = \frac{\partial x}{\partial t} = \pm 1/\sqrt{L_0C_0} = 1/\sqrt{\mu\epsilon} = c/\sqrt{\epsilon_r}$ and $Z_0 = \sqrt{L_0/C_0}$, which gives the result $T = 6L_0/r_s$. Using the previous formulae Kerkman et al. have calculated results for the dampening time and compared the results to actual measurements. The dampening time turns out to vary from several tens of microseconds up to several milliseconds. For example, for 150 meters of # 12-AWG bundled cable, the model gives a 3τ value of around 18 μs , which is close to the measured value of 20 μs . [22]

In a practical application of the suggested method it would be enough to measure the response of a pulse sent to the device and then determine the time it took for the resulting oscillation to decay under $< 5\%$ of the initial amplitude. This time could then be used in determining the minimum pulse width limitations for the configuration in question. If desired, the cable parameters could then be used to calculate the cable length or frequency of the oscillation.

Chapter 4

Modulation and pulse-width limitations

In chapter 3 the physical constraints determining the size of the MPW limitations were identified and discussed. However, the exact effect of the limitations on the modulation strategies and output of the modulator have not yet been discussed. This chapter discusses results obtained through the simulations and presents how the output of the modulator is changed by MPW limitations.

A simulator program was created in order to simulate the effect of minimum pulse-width limitations. The program modelled a real-time system commonly used in proprietary power converters. A simple inductive load was used to model the load in the system. The simple inductive load was enough, because the physical effects caused by the surrounding circuits were left out of this study. The simulator implements the different PWM methods discussed in chapter 2 and provides an interface to modify the MPW limitations and change the parameters of the simulation dynamically. This makes it possible to study the effects of MPW limitations and modulation methods on the pulse pattern in both time and frequency spaces.

As explained in chapter 2, the frequency response is important due to the introduced harmonics. Thus, responses in both the time and frequency

domains are considered. Aspects, such as voltage error produced by the MPW limitations and the effect on the pulse pattern are discussed. The pulse patterns shown in this chapter are shifted in y-direction to make it easier to distinguish between the three phases. In the actual calculations and applications all the pulses are of equal height and magnitude with no y-offset. In all figures the PWM signals for phases a, b and c are colored gray, green and purple respectively. The error signal is blue and the reference voltage signal is magenta. The signal amplitudes are out of proportion.

4.1 Time domain

Based on the discussion in chapter 2 one recalls that the calculated timing values for states yielded by equations 2.14 and 2.15 are subject to MPW limitations. These values reach their minima and maxima near the edges of the sectors of the SVM hexagon. From this it results that the pulse pattern is distorted near the edges of these sectors. Therefore, during transitions from one sector to another there is an error in the modulator output. The size of this error is proportional to the MPW limitations. This same phenomenon also introduces a condition called double switching, which happens when two of the three power poles are changing state simultaneously.

As we recall from chapter 2 the pulses, length of which is less than half of the minimum pulse width are dropped entirely while the longer pulses are held to match the limit. The opposing is true for the maximum pulse-width limit. The pulses, which are longer than the total switching cycle length minus half of the maximum pulse width are fused together. The pulses, which are longer than the maximum pulse width, but not as long as the fused pulses, are shortened to the maximum pulse width. This ensures that there is never a voltage transient, which the system cannot recover from before the next transient.

There are two possible methods of applying the pulse-width limitations in practice. The limitations can be applied directly to the calculated state

vector on times, which is trivial to implement in digital systems. However, this limits the system as a whole and removes a degree of freedom. It is also possible to apply the limits directly to the output signal of the modulator. However, this is arguably harder to implement in a digital system, because it is beneficial that the controller already knows the final lengths of the pulses in the waveform. Due to the nature of the PWM algorithm, the vector states are automatically known by the controller, but the actual realized waveforms are not realized until the signal is generated. Phase specific MPW limiting allows for smaller output signal distortion. However, the already calculated vector states are altered by this method creating possible discontinuities to the switching waveform.

4.1.1 Error caused by pulse-width limitations

During transitions from one SVM hexagon sector to the next, there is an error in the modulator output. This error originates from the handling of pulses shorter than the minimum pulse width or longer than the maximum pulse width.

The output signal error is apparent in figure 4.1. The figure shows the same modulation period with different MPW limitation settings using DPWM0 strategy using vector specific MPW limitations. It is clear that increasing the minimum pulse-width limitations also increases the relative size of the the error. The voltage error directly translates to distortion in the output signal, as the output signal no longer matches the commanded reference.

The distortion in the output PWM signal affects the output current of the device. In these simulations a simple inductive load was used to visualize how the current vector behaves in the d-q plane. Figure 4.2 presents the trajectory of the current vector, when DPWM2 modulation strategy is used. It is apparent that as the current vector passes from one SVM hexagon sector to another, there is distortion, size of which increases as the MPW limit increases.

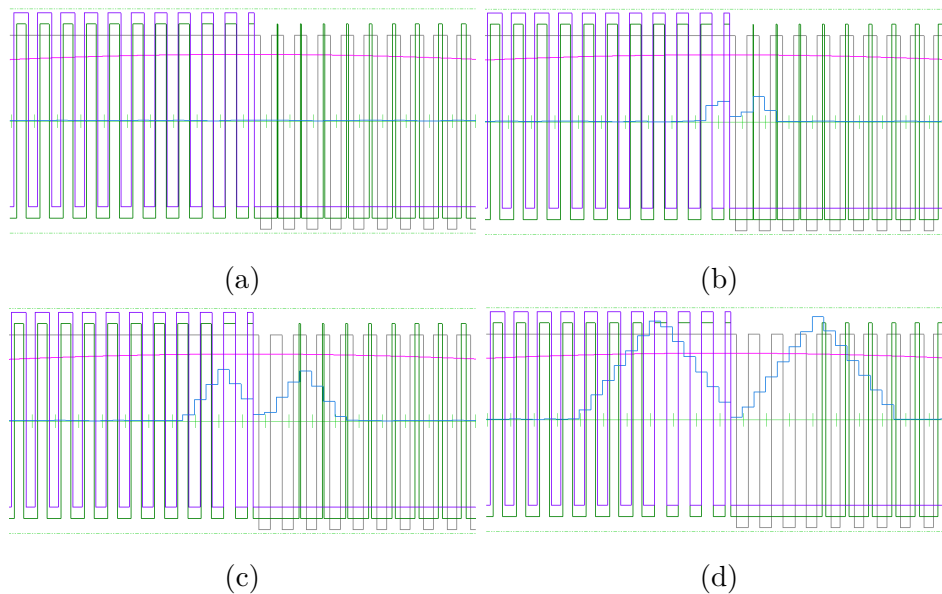


Figure 4.1: The switching waveform of DPWM0 strategy is presented with several vector specific MPW limitations. Figure 4.1a has no MPW limit; figure 4.1b has a MPW limit of $10 \mu s$; figure 4.1c has a MPW limit of $20 \mu s$ and figure 4.1d has a MPW limit of $40 \mu s$. The length of one switching cycle is $250 \mu s$ in all of the figures. It is clear that the amount of error in the output voltage increases as the MPW limits increase.

4.1.2 Choosing the modulation approach

In chapter 2 the differences between the various modulation strategies were discussed. However, the discussion deliberately skipped the effect of MPW limitations. Instead, the type of the load was given more focus. The simulations performed have shown how the effects of pulse-width limitations also depend on the modulation approach used.

One of the factors affecting the choice of modulation approach is distortion of the modulator output signal. All of the PWM methods have distortion at high modulation indices when the reference voltage vector is in the outer portions of the SVM hexagon. This fundamentally originates from the fact that SVM cannot realize a perfect circle for the trajectory of the reference vector after the SVM hexagon begins to clip this trajectory. The effect of

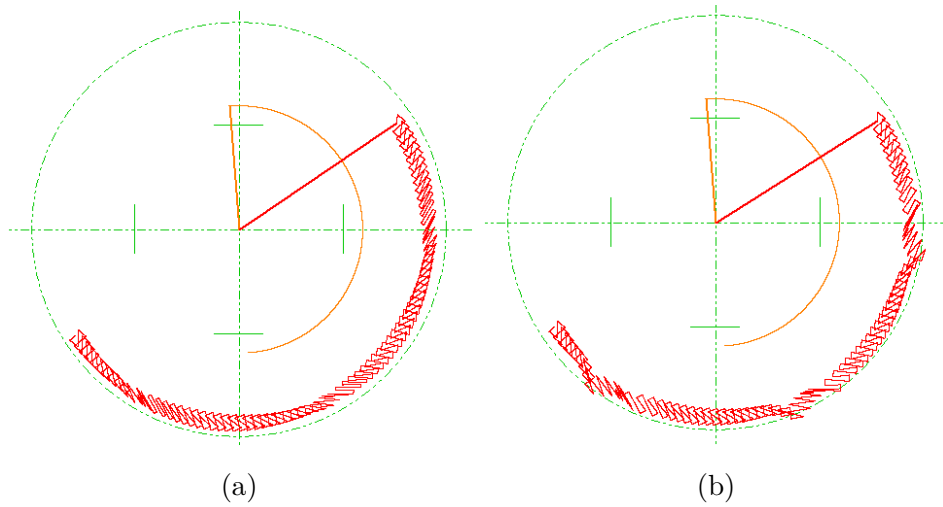


Figure 4.2: Pulse-width limitations distort the current vector trajectory. The trajectory of the current vector is shown in red and the trajectory of the reference voltage is shown in orange. Figure 4.2a represents the current trajectory of DPWM2 with $20 \mu s$ MPW limitation. The MPW limit is set to $40 \mu s$ in figure 4.2b. The length of one switching cycle is $250 \mu s$ in both figures.

MPW limitations and dead-time is taken in account when defining the size of the regions [3].

The continuous SVM has a distortion region, which is twice as large as that of the DPWM methods due to the fact that it has two zero vectors applied during each PWM cycle, whereas DPWM methods only apply one. However, the DPWM methods have additional distortion regions in different parts of the hexagon. The distortion regions are located between the hexagon sectors for DPWM0 and DPWM2. In the case of DPWM1 there are no distortion regions between the hexagon sectors, but only in the middle and on the outer edges of the hexagon. The distortion regions are depicted in figure 4.3. [3] The distortion regions depicted in this figure apply to the phase specific MPW limitations. Figure 4.4 presents how the distortion are visible in the switching waveform for DPWM0, DPWM1, DPWM2 and DPWM3. The vector specific MPW limitations always have symmetric distortion regions on both sides of the sectors.

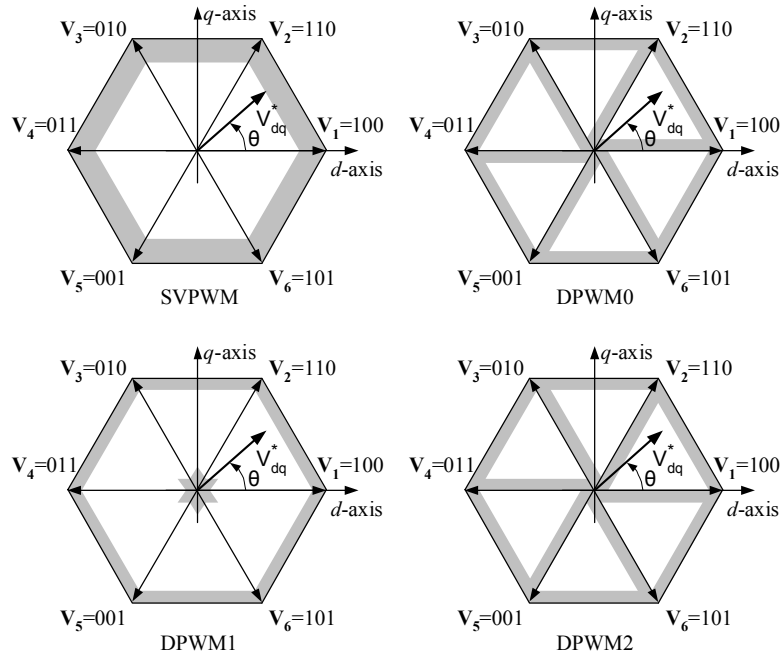


Figure 4.3: All of the PWM methods have distortion at high modulation indices. The distortion regions are different for each modulation method. The distortion region for SVPWM is twice as large as that of the discontinuous methods due to the application of two zero vectors during each PWM cycle. The worst case scenario is DPWM3 (not visible in the figure), distortion region of which is the overlap of the distortion regions of DPWM0 and DPWM2. [3]

The distortion regions play an important role in the selection of the modulation approach in the case of phase specific MPW limits. On one hand, SVPWM is the most suitable option for low modulation indices as there is no distortion in the middle of the hexagon. On the other hand, for high modulation indices the DPWM methods are always better. However, because DPWM0 and DPWM2 have distortion during sector changes it is beneficial to use DPWM1 during the transitions. This does not change the active voltage vector or increase the number of switching transitions as it merely selects a different zero vector. [3]

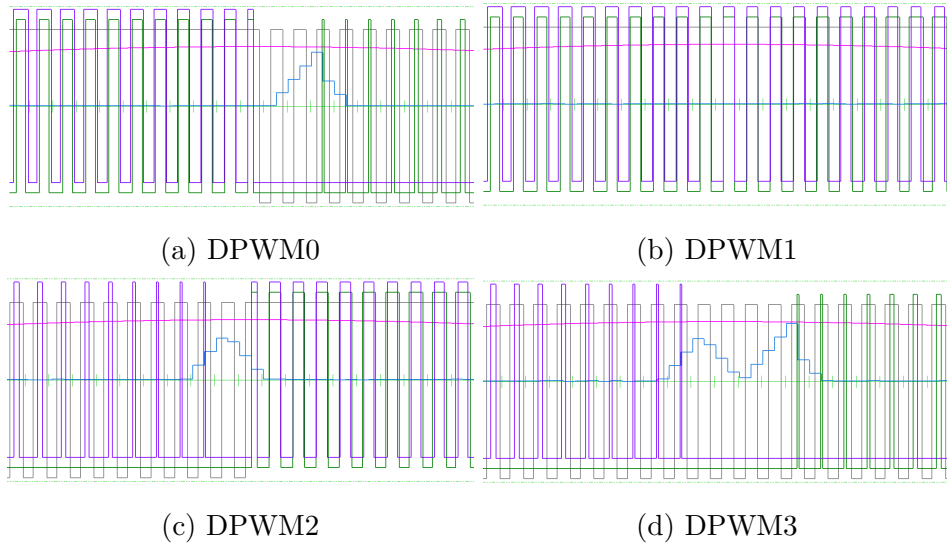


Figure 4.4: The distortion regions are clearly visible in the output error signal, when phase specific MPW limits are used. The used MPW limitation is $20 \mu s$.

4.1.3 Double switching

When the MPW limitations are in effect, the lengths of the pulses sent to the different phases can sometimes be equal and overlapping. As a result double switching occurs. Double switching is problematic, because the semi-conducting switches are not identical and cannot realize the voltage changes at the exact same time. This causes voltage spikes in the differential mode signal, which is unwanted, when the cable connecting the load to the power converter is long. In this case the voltage spikes cause strain on the insulation of the load, which effectively reduces its expected lifetime. An example of the double switching is presented in figure 4.5. On the right hand side of the figure the a and b phases are switched simultaneously due to MPW limitations.

Double switching can also induce non-linear effects. For instance, when the load is a motor, the simultaneous magnetization of two motor pole pairs results in non-linear behaviour. As a result a common mode zero current forms. The common mode current flows through bearings to the ground and

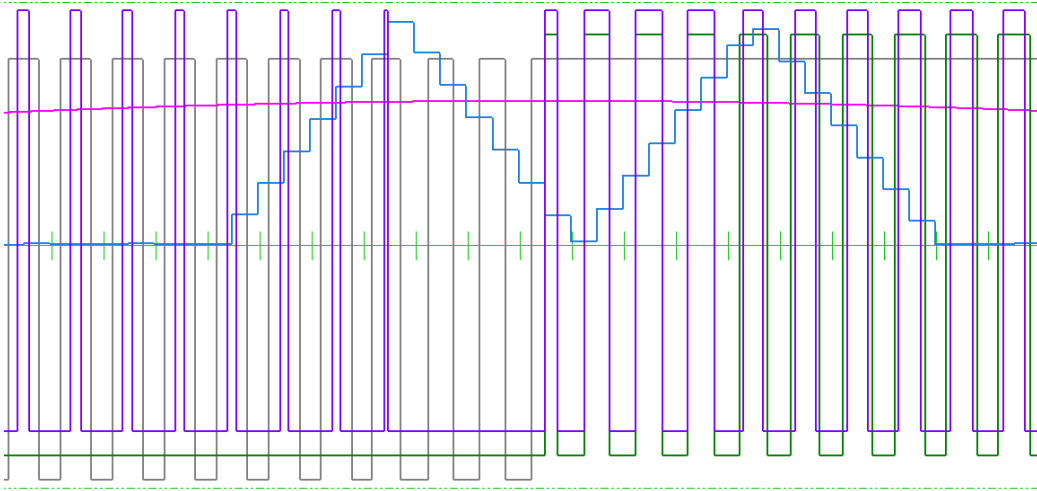


Figure 4.5: When MPW limitations are applied, double switching often occurs. This is apparent on the right side of the figure, where a and b phases are switched simultaneously. The figure is a 5 ms snippet of a DPWM2 simulation with MPW limitations set to 40 μ s, while switching cycle is 250 μ s.

reduces the life-time of the motor by wearing its bearings.

This thesis considers an open loop modulator, which limits the possible methods of handling the double switching issue. A possible way to reduce the double switching is to apply an offset to the pulse trains so, that during the MPW limitations they no longer overlap. The offset introduces a small phase error to the resulting phase currents. This results in an undesirable zero current. The effect of global offsetting on the spectrum is easy to determine using the well-known time shift property of Fourier transform $\mathcal{F}\{g(t - a)\} = e^{-i2\pi fa}G(f)$.

A further improvement on this idea applies the offsetting only during the MPW limitation zones, which reduces the zero current. However, applying the offset only during certain periods alters the original signal, which in turn results in a modified spectrum. Commercial power converters often utilize a closed loop controller to eliminate and compensate for double switching. The effect of the closed loop controller is the same as that of the localized pulse train offsetting around the MPW limitation zones.

The simulations have shown that DPWM3 does not suffer from double switching during the transitions, because the used zero vector is switched from \vec{U}_0 to \vec{U}_7 and vice versa in a suitable manner. Therefore, the zero vector choice after sector change eliminates the effect. Figure 4.6 shows the DPWM3 switching waveform during sector transit. It is interesting to note, that all other modulation strategies have double switching issues during sector transitions. The worst case scenario is DPWM1, which has twice the amount of double switching compared to the other modulation methods. However, as discussed earlier, DPWM3 suffers from distortion during the sector transitions. This results in a trade off between the elimination of double switching and achieving the least distorted output signal.

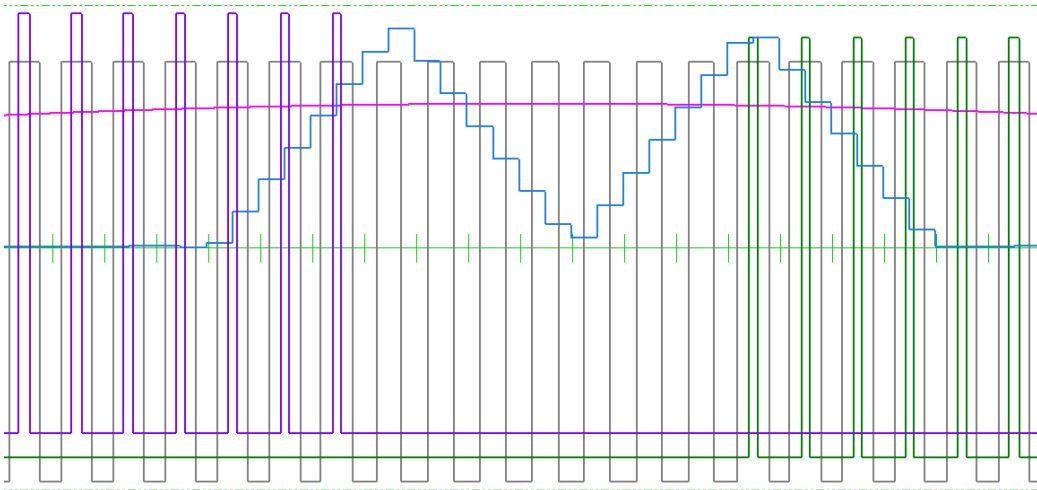


Figure 4.6: There is no apparent double switching in the simulation of DPWM3 modulation. The figure is a 5 ms snippet of a DPWM3 simulation with MPW limitations set to 40 μs , while switching cycle is 250 μs .

As suggested earlier, the switching of the modulation method dynamically can optimize the locations of the distortion regions. Additionally, switching to DPWM3 strategy during sector transitions eliminates the double switching problem. Inside the sectors the most optimal modulation strategy for the application can be used, as long as the strategy is changed to DPWM3 during sector transitions. This, however, can be more difficult to implement than

simple time offsetting. Figure 4.7 shows DPWM2 in sector transit with DPWM3 being applied, when MPW limitations are in effect. Note, that the figure is from the same position of the fundamental cycle, using the same modulation strategy and has the same MPW limits as figure 4.5.

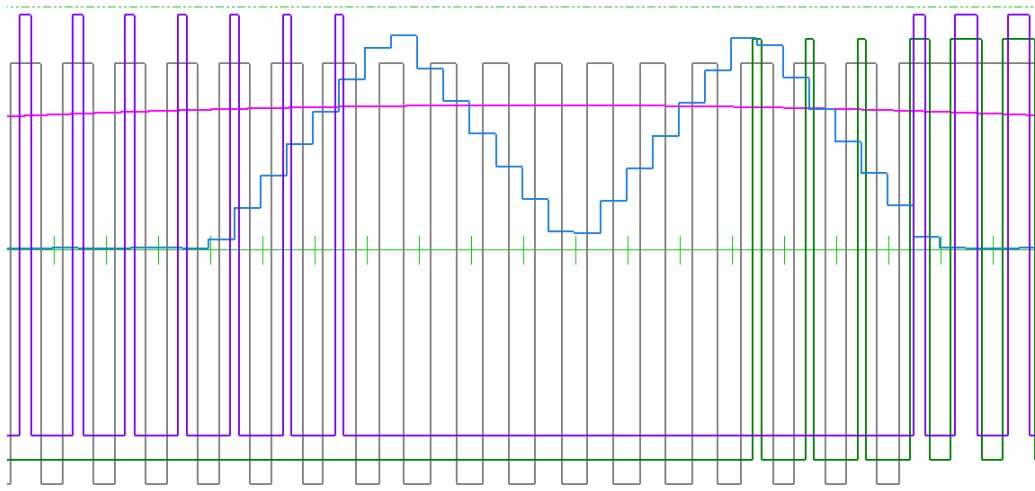


Figure 4.7: When DPWM3 strategy is used while the MPW limits are active, the double switching issue is eliminated. The figure is a 5 ms snippet of a DPWM2 simulation with MPW limitations set to 40 μ s, while switching cycle is 250 μ s.

4.1.4 Switching frequency

Enforcing the MPW limitations always results in dropped pulses, when the width of the pulses falls beyond certain limit. Therefore, while the switching frequency of the device is not physically changed by pulse-width limitations, the effective switching frequency is altered by them. The effective switching frequency can be measured by counting pulse edges during one or more full cycles of the fundamental. A straightforward representation of the effective switching frequency is a percentage of the original, non-limited, switching frequency.

Reducing the effective switching frequency results in decreased switching losses, because switching does not need to be performed for the dropped

pulses. Therefore, the change in effective switching frequency can be used as a meter to show how the limitations affect the accuracy and switching losses of the modulator.

This thought process results in a new possible method for increasing the efficiency of a power converter. In applications, where the output accuracy can be sacrificed, the MPW limitations can be deliberately set higher than actually determined by the physical system. This results in lower switching losses and, thus, improved efficiency.

Often switching losses are decreased by decreasing the switching frequency of the modulator. However, changing the switching frequency shifts the harmonic peaks of the spectrum of the output signal. Additionally, lower switching frequency results in less accurate control. Managing the switching losses using MPW limitations can therefore turn out to be beneficial.

4.2 Output voltage spectrum

Applying MPW limits changes the output signal and therefore also affects the spectrum of the signal. Determining how the spectrum of the signal changes is important as the new harmonics introduced may result in increased common mode current or require additional EM shielding. The filters used in the device may also need to be optimized for the spectrum. Determining the harmonic response was discussed earlier in this thesis.

For the purposes of this thesis, the switching waveform generated by the simulator program is exported and then imported into Matlab. The imported data is then converted to frequency space using Fourier transform. Basic rectangular window is used in the conversion, because the dataset is ensured to be continuous by both the simulation and the post processing performed. The converted data is then finally analysed. Common mode voltage has been subtracted from the measurements. The used switching frequency is 4 kHz and the fundamental frequency is 50 Hz. It turns out, that the shape of the envelope function of the spectrum and the shapes of the individual harmonics

are well predicted by the analytic discussion in chapter 2.

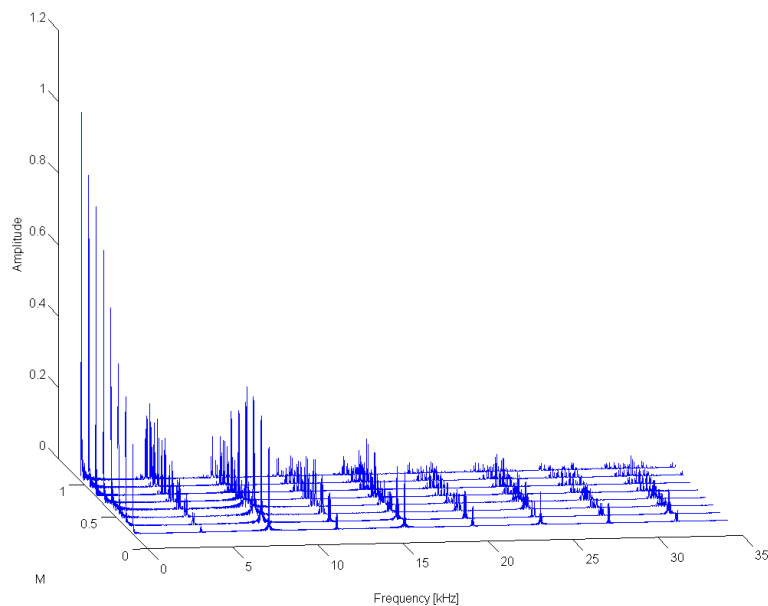
4.2.1 Modulation strategy and index

Reviewing equation 2.21 and assuming that the derivation process stays fundamentally similar for other types of modulation algorithms, it is possible to deduce that the modulation index is a major factor in determining the heights of the individual harmonic spikes. The modulation index M is the sole factor determining the shape of the Bessel function envelope of the harmonic response in equation 2.21.

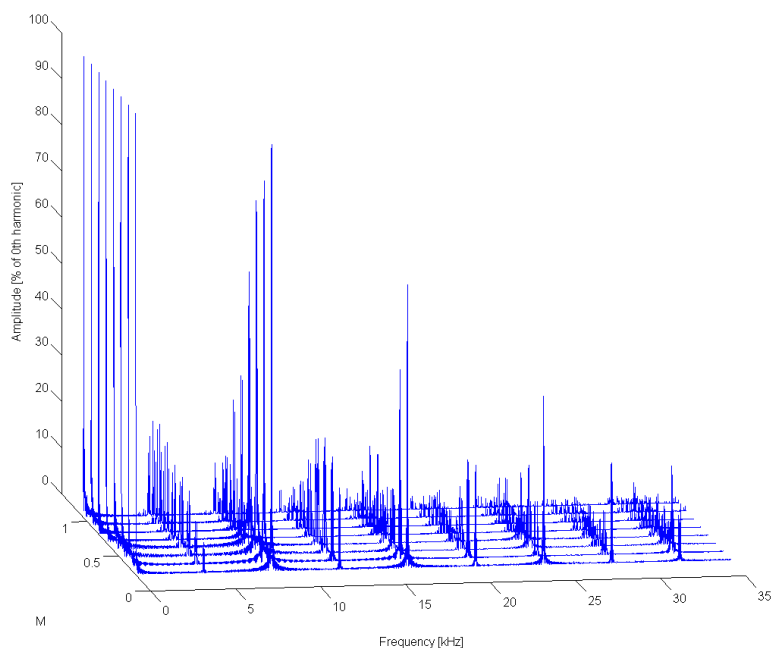
The above assumption can be verified by studying the harmonic responses of the simulation results. When studying the measured harmonic responses, the modulation index indeed turns out to be the most determining factor for the height and shape of the harmonic spikes. For reference, the change of the spike heights in the case of SVPWM with no MPW limitations is shown in figure 4.8. The figure presents the spectrum of phase voltage with the effect of common mode voltage removed. The spectrum spikes are well aligned considering the switching frequency of 4 kHz and fundamental frequency of 50 Hz.

The effect of modulation index on the harmonic response is important, because the filters used in the power converter must be designed so that they work even when the modulation index is varied. The varying modulation index is thus yet another variable to be considered when designing commercial solutions. The modulation index stays as the determining factor for the amplitude of the spikes in all modulation strategies, however, the amplitudes are not identical between the different modulation strategies.

The modulation strategy has a major effect on the spike shape and amplitude in the spectrum. Figure 4.9 presents an overview of the different strategies for switching frequency of 4 kHz, fundamental frequency of 50 Hz and modulation index of 0.59. When studying the figure, it becomes apparent that the discontinuous modulation strategies can be grouped together. Clearly the spectra of both DPWMMIN and DPWMMAX are almost identi-



(a)



(b)

Figure 4.8: The modulation index is a major factor determining the amplitude of the peaks in the spectrum of the switching waveform for phase voltage. Figure 4.8a presents how the modulation index affects the shape and the amplitude of the spikes in the spectrum for the continuous SVPWM strategy. Figure 4.8b presents the spectrum amplitudes relative to the 0th harmonic.

cal. Similarly DPWM0 and DPWM2 form a pair and DPWM1 and DPWM3 share similarities. This is to be expected due to symmetry; it turns out DPWMMIN and DPWMMAX are essentially the same, the zero vectors are simply interchanged. The same applies for the two other identified pairs. It is possible to convert them to one another by swapping the used zero vectors. Another interesting phenomenon is the behaviour of the width of the spikes: in the discontinuous methods, where the used zero vector is altered periodically, there is apparent widening of the spikes.

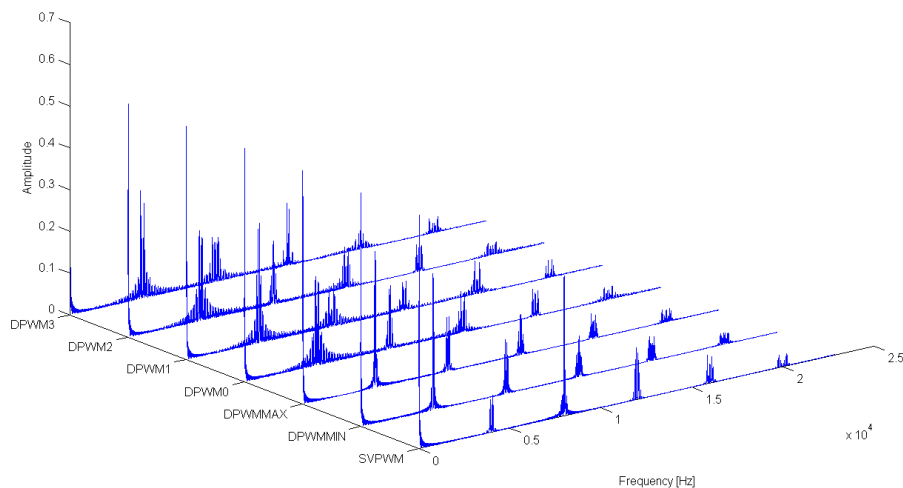


Figure 4.9: Different modulation strategies have different spectra. This figure presents how the modulation strategy affects the shape and the amplitude of the spikes in the frequency response. Common mode voltage has been subtracted from the measurements. The modulation index is 0.59.

The modulation index still has an effect on the harmonic spectra of the modulation strategies. This response is presented in figure 4.10. It is apparent, that the harmonics of different modulation strategies react differently to the changes in the modulation index. For instance the 1st harmonic peak of the carrier tends to be slightly higher with DPWM1 and DPWM3 strate-

gies when compared to DPWM0 and DPWM2, whereas the 2nd harmonic peak tends to behave in an opposite manner. The differences, however, are surprisingly small and the effect of the modulation index on the spectrum of discontinuous methods is far smaller than that on the continuous method.

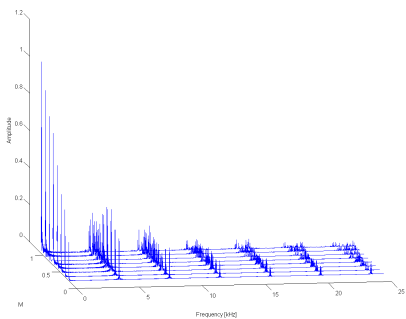
4.2.2 Pulse-width limitations

The effect of pulse-width limitations on the spectrum is difficult to determine analytically. However, a qualitative hypothesis on the behaviour can be achieved by assuming that MPW limitations cut the resulting waveform so that perfect sinusoidal no longer forms. This gives the intuitive hypothesis that the spikes of the spectrum of the switching waveform widen.

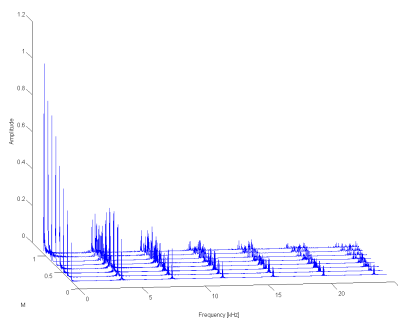
When measurements are performed in the case of vector specific MPW limitations, the above hypothesis appears to be true. Figure 4.11 presents spectrum of the DPWM2 switching strategy with modulation index at 0.59, switching frequency at 4 kHz and fundamental frequency at 50 Hz with common mode voltage subtracted. It is clear, that as the vector specific MPW limits increase, there is an apparent widening in the spikes of the spectrum. The widening, however, turns out to be relatively subtle and is most visible on the 2nd harmonic of the carrier. When a similar analysis is performed on the common mode component only, there is also only a subtle widening in the spikes of the spectrum as well.

Measurements show that the widening behaviour persists at higher modulation indices. With large modulation indices the distortion in the output signal is stronger. Therefore the width of the spectrum peaks grows more at large modulation indices than with smaller modulation indices as pulse-width limitations increase.

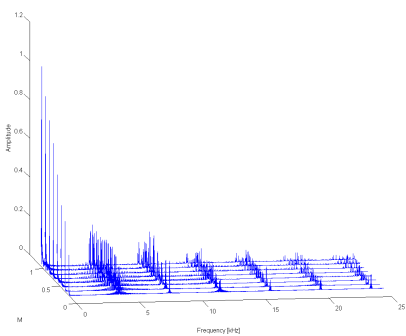
As MPW limitations increase, additional low frequency spikes in the spectrum appear. Figure 4.12 presents this phenomenon in the case of vector-specific MPW limitations and 4.13 presents it in the case of phase-specific MPW limitations. The spikes originate from the discontinuities that form, when the signal is clipped due to the MPW limitations. It is interesting



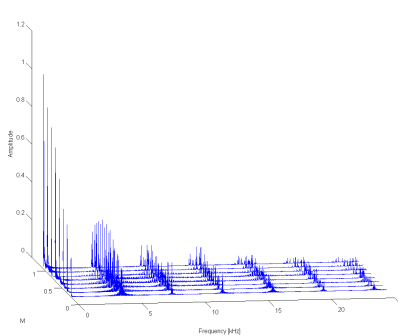
(a) DPWMMIN



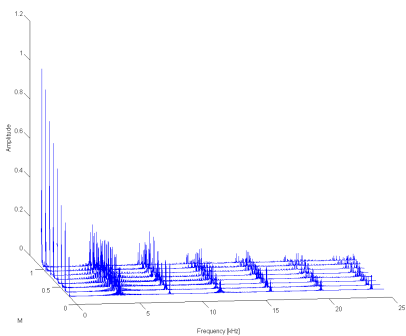
(b) DPWMMAX



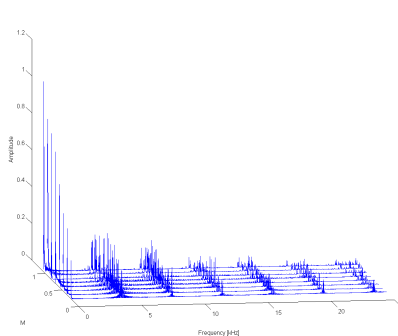
(c) DPWM0



(d) DPWM1



(e) DPWM2



(f) DPWM3

Figure 4.10: The spectrum of different modulation strategies is presented for a set of modulation indices. The similarities in the pairs DPWMMIN-DPWMMAX, DPWM0-DPWM2 and DPWM1-DPWM3 are obvious. Common mode voltage has been subtracted from the measurements.

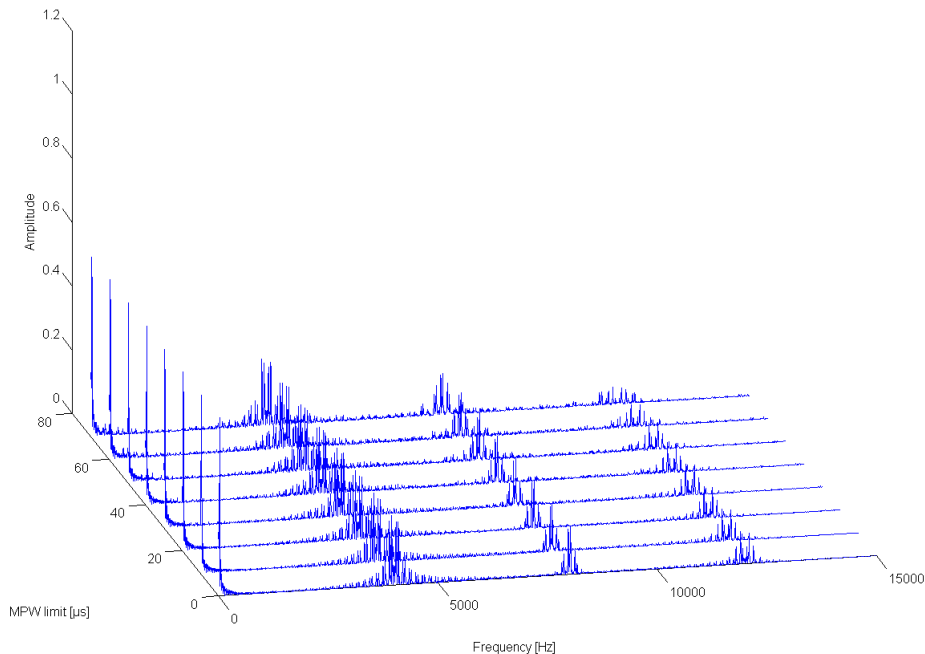


Figure 4.11: Pulse-width limitations affect the width of the spikes in the spectrum of the switching waveform. Common mode voltage has been subtracted from the measurements. The modulation index is 0.59 and the modulation strategy used is DPWM2.

to note how there is a local maximum of the envelope function near 1 kHz. For the 10 μs case the maximum is not visible, but it begins to appear in the 30 μs case. Finally it becomes a dominating feature in the 40 and 50 μs cases. The magnitude of the spikes, when phase-specific limitations are used, is smaller than when the vector-specific limitations are used. However, in the former case the spikes exist at much lower frequencies. The lowest frequency spike in the case of phase-specific limitations is located near 250 Hz, while it is located near 400 Hz in the case of vector-specific limitations.

The formation of the low frequency spikes is undesired, as the LC-filter connected to the output of the power converter is tuned to a specific frequency. If the appearance of these spikes has not been taken in account,

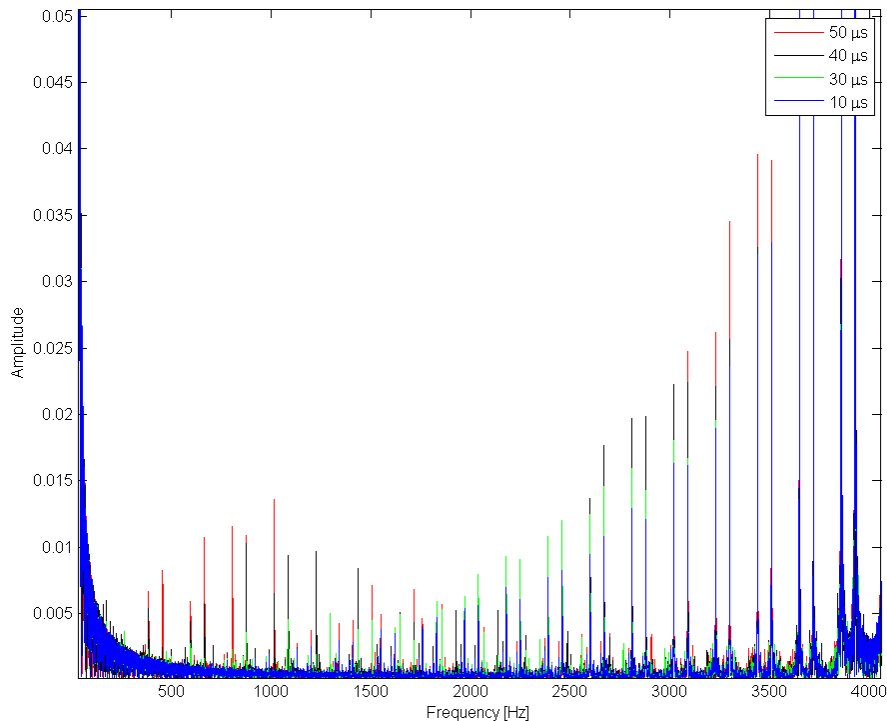


Figure 4.12: As vector specific MPW limitations increase, additional low frequency spikes in the spectrum appear. Common mode voltage has been subtracted from the measurements. The modulation index is 0.82 and the modulation strategy used is DPWM2.

when the filter was designed, the output signal of the power converter deteriorates as MPW limits are introduced. It is interesting to note, that these peaks happen at multiplies of the frequency of the fundamental.

4.2.3 Double switching elimination

The previously suggested dynamic switching of modulation strategy in order to eliminate the double switching issue changes the switching waveform near SVM hexagon sector transits. Therefore, changes to the resulting spectrum are expected. Figure 4.14 presents the spectrum of DPWM2 with dynamic

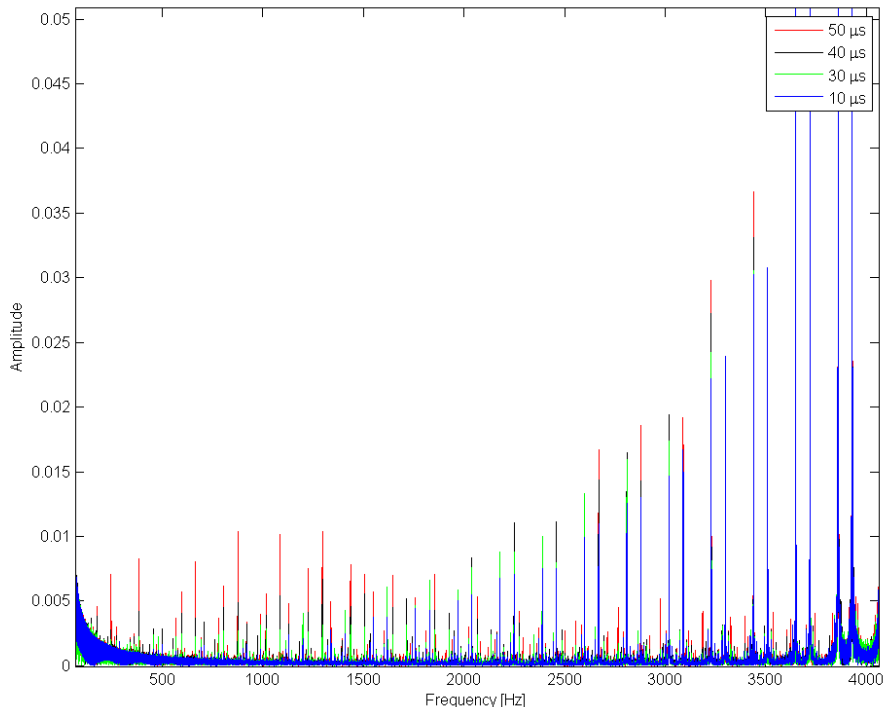


Figure 4.13: As phase specific MPW limitations increase, additional low frequency spikes in the spectrum appear. Common mode voltage has been subtracted from the measurements. The modulation index is 0.82 and the modulation strategy used is DPWM2.

switching of modulation strategy at different MPW limits. Otherwise the same configuration is used as for figure 4.11. This allows for easy comparison of the two cases. The dynamic switching of modulation strategy has no effect on the behavior of the low frequency spikes as shown in figure 4.15. However, the narrower envelope function of the 1st harmonic spike is also visible on this figure.

When the two figures are compared, it becomes clear that the spectrum in 4.14 suffers from less widening in the cases of the 1st and 3rd harmonics than the spectrum in 4.11. However, there is apparent widening in the 2nd harmonic. However, the DPWM3 strategy used during the transits has a

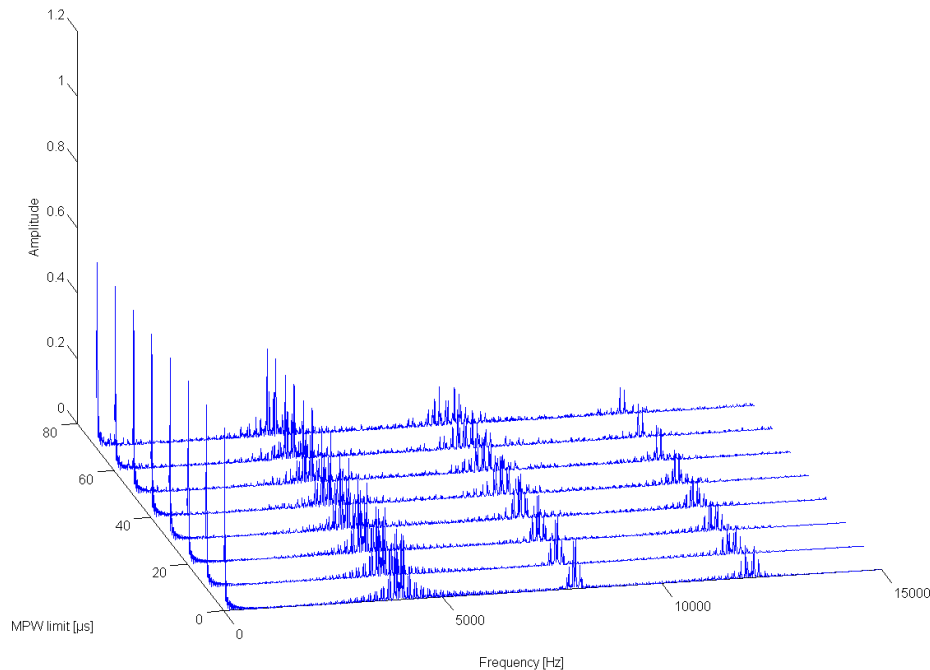


Figure 4.14: This figure presents how pulse-width limitations affect the width of the spikes in the spectrum of the switching waveform when the suggested double switching elimination strategy is used. Common mode voltage has been subtracted from the measurements. The modulation index is 0.59 and the modulation strategy used is DPWM2.

distortion region in the middle of the hexagon making this strategy perform less well for small modulation indices, when SVPWM is used.

Based on the analysis is therefore suggested by the author that the dynamic selection of switching strategy is used in the case of vector specific MPW limitations. It results in both good harmonic performance and elimination of the double switching phenomenon. Both of these are sought after traits in power converters.

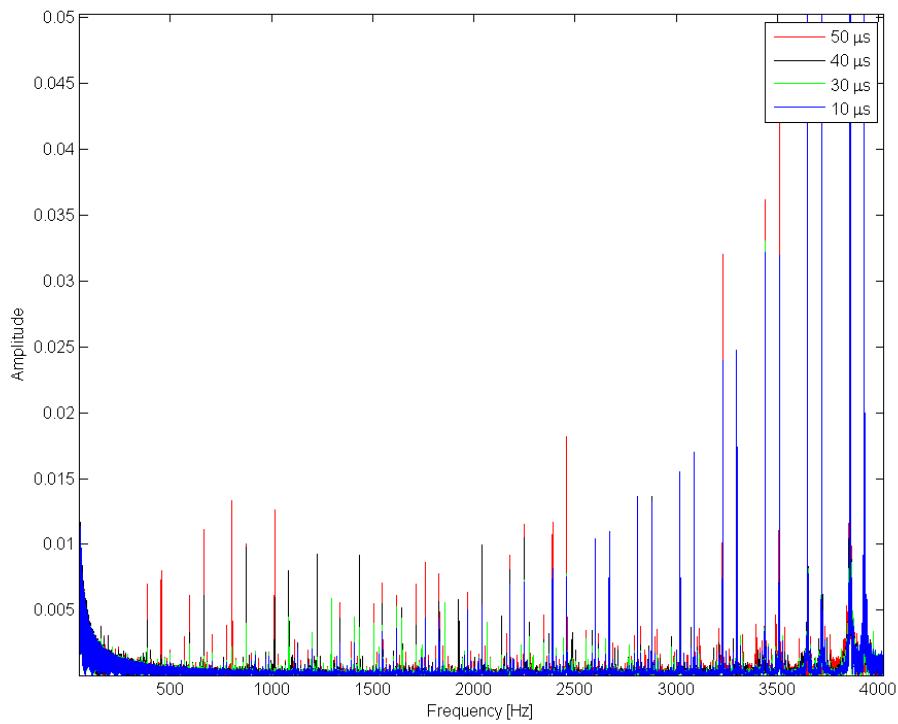


Figure 4.15: The double switching elimination has no visible effect on the behavior of the low frequency spikes. Common mode voltage has been subtracted from the measurements. The modulation index is 0.82 and the modulation strategy used is DPWM2.

Chapter 5

Conclusions

This thesis first reviewed the different modulations methods used in power converters. Then it introduced the MPW limitations and discussed the physical constraints determining them. The effect of the MPW limitations on the modulation methods was finally simulated and the results of the simulations were analysed.

As discussed in chapter 3, the MPW limitations are determined by a multitude of factors. How the factors contribute to the MPW limitations is unique to each power converter design and depend on the components used. However, it is obvious that the limitations can be divided into two categories. The first category containing those factors built-in to the converter and the second category containing the external factors. In industrial applications, the author recommends that these categories are considered separate if possible. This allows the power converter to have built-in MPW limitations for the design and further limitations can be programmed based on the external components. In future, the power converter software could determine the effect of the load and cable oscillations and adjust the MPW limitations accordingly.

In chapter 3 the problem of larger than two times the power unit voltage pulses was identified. It was reasoned that the problem can be prevented by determining the pulse-width limitations in the case of long motor cables. A

method for calculating the required pulse-width limitations was presented. The measurement of the reflecting pulse turned out to be possible with the current hardware of power converters, allowing for interesting new features. Such as calculating the length of the motor cable from user defined parameters.

In chapter 4 it became apparent that the MPW limitations have a large effect on the output of the modulator. The effect of the limitations was researched in both time and frequency domains. Two possible ways of limiting the pulse-width were introduced: the vector-specific method and the phase-specific method. Double switching resulting from the application of MPW limitations was identified and determined to be a critical issue in the case of long motor cables and vector-specific MPW limitations. An offsetting of the pulse-trains either globally or locally during the limitation areas was suggested as a remedy to the problem. A more sophisticated way of handling the double switching issue by dynamically changing the modulation strategy was also suggested and demonstrated in practice. The dynamic switching of the modulation strategy was found to have no major side-effects.

It was suggested that in the case of long motor cables the vector specific MPW limitations are used and phase specific MPW limitations are used in the case of short cables. This allows for avoiding the double switching issue in the case of long cables. Changing the modulation strategy dynamically in order to achieve least distortion in the output signal was also discussed. However, this turned out to result in a trade off between reaching lowest possible distortion and the elimination of double switching.

The spectrum of the switching waveform was studied and the factors determining the shape of the spectrum were identified. The effect of the MPW limits on the spectrum when deep in the linear modulation region was found to be rather minuscule, although the widening of the spikes in the spectrum was clearly visible. It was noted that at higher modulation indices the widening behaviour is stronger. The effect of the suggested double switching elimination strategy on the spectrum was also studied. The strategy turned

out to have no major negative impacts on the spectrum. Instead the 1st and 3rd harmonics of the carrier were narrower using this strategy, and only the 2nd harmonic of the carrier widened. The low frequency spectrum was also studied and the behaviour of the harmonics of the fundamental was discussed.

The effect of MPW limitations on the effective switching frequency was discussed and it was suggested that the limitations could be used to control the efficiency of the device by trading accuracy of the output to decreased switching losses.

Bibliography

- [1] D. Holmes and T. Lipo, *Pulse Width Modulation for Power Converters: Principles and Practice*. John Wiley & Sons, 2003.
- [2] N. Mohan, *Power Electronics: A First Course*. John Wiley & Sons, 2012.
- [3] B. Welchko, S. Schulz, and S. Hiti, “Effects and compensation of dead-time and minimum pulse-width limitations in two-level pwm voltage source inverters,” in *Industry Applications Conference, 2006. 41st IAS Annual Meeting. Conference Record of the 2006 IEEE*, vol. 2, Oct 2006, pp. 889–896.
- [4] K. Zhou and D. Wang, “Relationship between space-vector modulation and three-phase carrier-based pwm: A comprehensive analysis,” *IEEE Transactions on Industrial Electronics*, vol. 49, no. 1, pp. 186–196, 2002.
- [5] M. Norrkniivilä, “Voltage orientation based control method for the rotor flux and torque of the squirrel-cage induction machine,” Master’s thesis, Helsinki University of Technology, 2000.
- [6] H. van der Broeck, H.-C. Skudelny, and G. Stanke, “Analysis and realization of a pulsewidth modulator based on voltage space vectors,” *IEEE Transactions on Industrial Applications*, vol. 24, no. 1, pp. 142–150, 1988.
- [7] B.-H. Kwon, T.-W. Kim, and J.-H. Youm, “A novel svm-based hysteresis

- current controller,” *IEEE Transactions on Power Electronics*, vol. 13, no. 2, pp. 297–307, 1998.
- [8] M. Żelechowski, “Space vector modulated - direct torque controlled(dtc - svm) inverter - fed induction motor drive,” Ph.D. dissertation, Warsaw University of Technology, 2005.
- [9] S. Bowes and B. Bird, “Novel approach to the analysis and synthesis of modulation processes in power convertors,” *Proceedings of the Institution of Electrical Engineers*, vol. 122, no. 5, pp. 507–513, 1975.
- [10] B. J. Baliga, *Advanced Power MOSFET Concepts*. Springer, 2010.
- [11] M. Azuma and M. Kurata, “Gto thyristors,” *Proceedings of the IEEE*, vol. 76, no. 4, pp. 419–427, 1988.
- [12] P. Steimer, H. Gruning, J. Werninger, E. Carroll, S. Klaka, and S. Linder, “Igtc-a new emerging technology for high power, low cost inverters,” *IEEE Industry Applications Magazine*, vol. 5, no. 4, pp. 12–18, 1999.
- [13] M. Rashid, *Power electronics handbook: devices, circuits, and applications*. Elsevier, 2011.
- [14] J. Niiranen, *Tehoelektroniikan Komponentit*. Otatieto, 2007.
- [15] B. Williams, *Power Electronics: Devices, Drivers, Applications, and Passive Components*. Barry W. Williams, 2006.
- [16] L. Chen, “Intelligent gate drive for high power mosfets and igbts,” Ph.D. dissertation, Michigan State University, 2008.
- [17] M. Nguyen, R. Cassel, and G. Pappas, “Gate drive for high speed, high power igbts,” in *Pulsed Power Plasma Science, 2001. PPPS-2001. Digest of Technical Papers*, vol. 2, Jun 2001, pp. 1039–1042.
- [18] H. Sarén, “Analysis of the voltage source inverter with small dc-link capacitor,” Ph.D. dissertation, Lappeenranta University of Technology, 2005.

- [19] K. Pietiläinen, L. Harnefors, A. Petersson, and H.-P. N, “Dc-link stabilization and voltage sag ride-through of inverter drives,” *IEEE Transactions on Industrial Electronics*, vol. 53, no. 4, pp. 1261–1268, 2006.
- [20] H. Beukes, J. Enslin, and R. Spee, “Busbar design considerations for high power igbt converters,” in *Power Electronics Specialists Conference, 1997. PESC '97 Record., 28th Annual IEEE*, vol. 2, Jun 1997, pp. 847–853.
- [21] A. Tarkiainen, “Motor cable oscillations in electric drives,” Master’s thesis, Lappeenranta University of Technology, 1999.
- [22] R. Kerkman, D. Leggate, and G. Skibinski, “Interaction of drive modulation and cable parameters on ac motor transients,” *IEEE Transactions on Industry Applications*, vol. 33, no. 3, pp. 722–731, 1997.
- [23] S. Amarir and K. Al-Haddad, “A modeling technique to analyze the impact of inverter supply voltage and cable length on industrial motor-drives,” *IEEE Transactions on Power Electronics*, vol. 23, no. 2, pp. 753–762, 2008.
- [24] J. Lielpeteris and R. Moreau, *Liquid Metal Magnetohydrodynamics*. Kluwer Academic Publishers, 1989.
- [25] W. Duesterhoeft, M. Schulz, and E. Clarke, “Determination of instantaneous currents and voltages by means of alpha, beta, and zero components,” *Transactions of the American Institute of Electrical Engineers*, vol. 70, no. 2, pp. 1248–1255, 1951.
- [26] R. Park, “Two-reaction theory of synchronous machines generalized method of analysis-part i,” *Transactions of the American Institute of Electrical Engineers*, vol. 48, no. 3, pp. 716–727, 1929.

Appendix A

Park's transform

The highly coupled nature of inverter loads such as induction and synchronous machines has led to the use of artificial variables rather than actual variables for the purpose of simulation and visualization. In essence the Park's transform (or dqo-transform) is based on the assumption that the sum of the three currents in a three-phase system sum to zero. In this case the stator current vector is constrained to exist only on a plane defined by

$$i_a + i_b + i_c = 0. \tag{A.1}$$

This equation defines a general plane in a 3-dimensional space and is called the d-q plane. Components of the current and voltage vector in the plane are called the d-q components while the component in the axis normal to the plane is called the zero component $e_i(t)$. This zero component exists in the event that the currents do not sum to zero. [1]

In order to consider Park's transform one must first understand the concept of Clarke transform, also known as the alpha-beta transform. Clarke transform is the projection of the three phase quantities onto two stationary axes. There are two version of this transform. In the first one the transform is not unitary and hence the active and reactive powers in the resulting domain are not the same as those in the standard frame of reference. In the second version the matrix is unitary, however, in this case the amplitudes of the transformed quantities are not the same as in the standard frame of

reference. The non-invariant transform is presented in equation A.2 and the invariant transform is presented in equation A.3. This transform places the new γ -axis an equal distance away from all three of the original a, b, and c axes. In a balanced system, the values on these three axes would always balance each other in such way that the γ -axis value would be zero. [25]

$$i_{\alpha\beta\gamma}(t) = Ti_{abc}(t) = \frac{2}{3} \begin{pmatrix} 1 & -\frac{1}{2} & -\frac{1}{2} \\ 0 & \frac{\sqrt{3}}{2} & -\frac{\sqrt{3}}{2} \\ \frac{1}{2} & \frac{1}{2} & \frac{1}{2} \end{pmatrix} i_{abc}(t) \quad (\text{A.2})$$

$$i_{\alpha\beta\gamma}(t) = Ti_{abc}(t) = \sqrt{\frac{2}{3}} \begin{pmatrix} 1 & -\frac{1}{2} & -\frac{1}{2} \\ 0 & \frac{\sqrt{3}}{2} & -\frac{\sqrt{3}}{2} \\ \frac{1}{\sqrt{2}} & \frac{1}{\sqrt{2}} & \frac{1}{\sqrt{2}} \end{pmatrix} i_{abc}(t) \quad (\text{A.3})$$

In electric systems the values of a, b and c are oscillating in such way that the net vector is spinning. Park's transform extends Clarke transform so, that this effect is removed. In a balanced system, the vector is spinning around the γ -axis. Hence a rotation around this axis is applied to the Clarke transform. This yields the following result in the non-invariant case. The calculation is trivial to repeat for the invariant case.

$$\begin{aligned} & \frac{2}{3} \begin{pmatrix} \cos(\theta) & \sin(\theta) & 0 \\ -\sin(\theta) & \cos(\theta) & 0 \\ 0 & 0 & 1 \end{pmatrix} \begin{pmatrix} 1 & -\frac{1}{2} & -\frac{1}{2} \\ 0 & \frac{\sqrt{3}}{2} & -\frac{\sqrt{3}}{2} \\ \frac{1}{2} & \frac{1}{2} & \frac{1}{2} \end{pmatrix} = \\ & \frac{2}{3} \begin{pmatrix} \cos(\theta) & \cos(\theta - \frac{2\pi}{3}) & \cos(\theta + \frac{2\pi}{3}) \\ -\sin(\theta) & -\sin(\theta - \frac{2\pi}{3}) & -\sin(\theta + \frac{2\pi}{3}) \\ \frac{1}{2} & \frac{1}{2} & \frac{1}{2} \end{pmatrix} \end{aligned} \quad (\text{A.4})$$

After this transform the rotated α , β , and γ axes are commonly called d, q and o, where d comes from the word direct, q from the word quadrature and o stands for the zero axis or the zero component. The final transform can then be thought of as the projection of the three separate sinusoidal phase quantities onto two axes rotating with the same angular velocity as the sinusoidal phase quantities. While the representation Park gave for this

transform is slightly different than the one given above, the transform is still widely known as Park's Transform. Park originally presented the transform only for the non-invariant case. [26]